Nonidet P-40, 50% glycerol, and 2 mM each dNTP (TaKaRa, Shiga, Japan) with 6.0 pmol of Cy3-labeled ED-1 (Cy3–ED-1), 6.0 pmol of Cy5-labeled ED-2 (Cy5–ED-2), 30 fmol each of the 96 D1s, and 1.5 U *Ex Taq* polymerase. The reaction initially was incubated at 95 °C for 1 min, followed by 30 cycles of 95 °C for 30 s, 55 °C for 6 min, and 72 °C for 30 s, using a Bio-Rad PTC-200 Peltier thermal cycler. The reaction was stopped by holding the temperature at 10 °C.

Hybridization and detection on DNA microarray

We purchased a DNA microarray (NovusGene, Tokyo, Japan) that had 24 separated areas on the same slide glass. Each of the separated areas contained 100 types of oligonucleotide probe (96 probes for 96 SNPs and 4 probes for validation controls of the assay) identical to D1 sequences. Of the 4 validation control probes, 3 were not used in the DigiTag2 assay because these probes were prepared to validate the washing step with magnetic beads in the previous version of the DigiTag assay. The ready-to-use DNA microarrays were stored in a desiccator at room temperature until use.

A hybridization mixture was prepared by mixing 5 µl of labeled products in 12 µl of hybridization buffer containing 0.5× SSC, 0.1% sodium dodecyl sulfate (SDS), 15% formamide, and 1 mM EDTA with 1 µl of hybridization control. The hybridization control was prepared with 2.5 fmol of Cy3-labeled D1_100 and Cy5-labeled D1_100. Then 8 µl of the hybridization mixture was applied to each area on the DNA microarray. Hybridization was carried out for 30 min at 37 °C in a hybridization oven (ThermoStat plus, Eppendorf, Hamburg, Germany). After hybridization, DNA microarrays were washed in washing buffer (0.1× SSC and 0.1% SDS) with shaking at 60 rpm for 5 min. DNA microarrays were consecutively washed in distilled water with shaking at 60 rpm for 1 min and were then dried by centrifugation at 2000 rpm for 1 min. Hybridization images were scanned at photomultiplier voltages of 400 V for Cy3 and 480 V for Cy5 using a commercially available DNA chip scanner, and fluorescence image analysis was performed using commercially available software (GenePix 4000B unit and GenePix Pro 4.1 software package, Axon Instruments, Foster City, CA, USA). The genotype calls were determined using the SNPStar software (version 0.0.0.8, Olympus, Tokyo, Japan).

Results and discussion

DigiTag2 assay scheme

We previously reported a multiplex SNP typing method, the DigiTag assay, in which all of the SNP genotypes are encoded to the well-designed oligonucleotides, named DNA coded numbers (DCNs) [20]. The assignment of the DCNs to the SNPs is unconstrained; therefore, the DNA chips prepared to read out the types of DCN are universally available for any types of SNP. We revealed that the DigiTag assay has the potential to analyze nearly all kinds of SNP with high accuracy and reproducibility. However, the DigiTag assay needs the washing step with magnetic beads, which is a laborious step in manipulation. Also, the biotinylated probes, which are necessary for the washing step, are expensive. For the next version of the assay, we improved the protocol to exclude the washing step and named it the DigiTag2 assay.

The DigiTag2 assay involves four steps to accomplish the genotyping: target preparation, encoding, labeling, and detection (Fig. 1). During target preparation, target fragments (including target SNP sites) are prepared by multiplex PCR from genomic DNA. For multiplex PCR, we designed 40-mer primers (average length) and performed multiplex PCR using a two-step protocol (denature and extension steps) with a 6-min extension step. For encoding, we prepared two 5′ query probes and one 3′ query probe for each SNP site. The 5′ query probes have a sequence

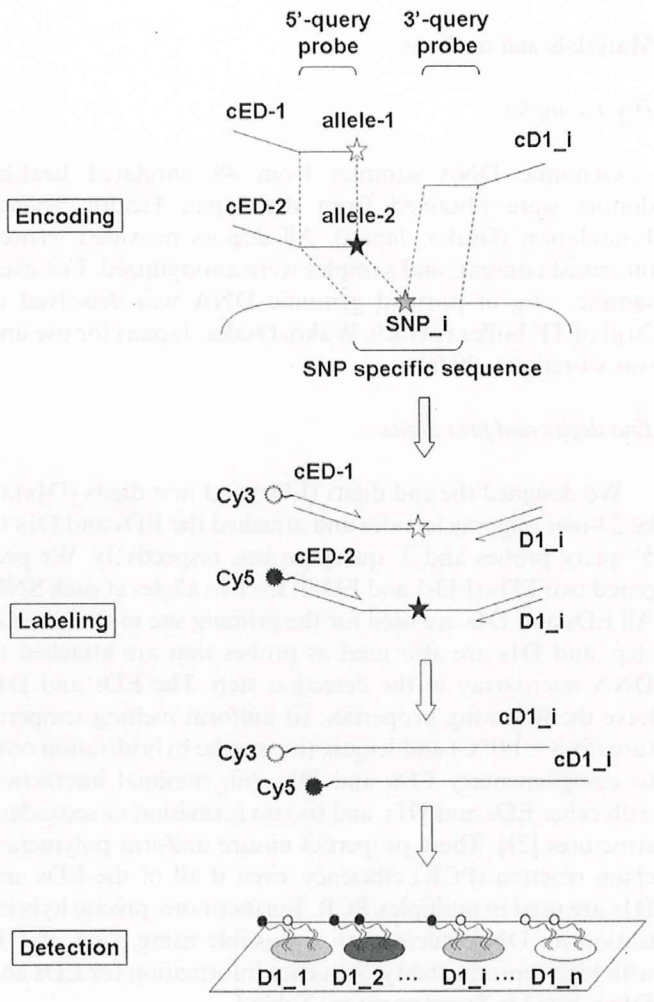

Fig. 1. Schematic representation of DigiTag2 assay. This assay involves four steps to accomplish SNP typing: target preparation, encoding, labeling, and detection. The 5′ query probes have EDs (cED-1 and cED-2) corresponding to each allele, and the 3′ query probes have a variable sequence (cD1_i) for each SNP. Each reverse complement sequence is depicted by a lowercase "c" before the sequence name.

complementary to the 5′-flanking region of the target SNP, and each of the probes has an allele-specific sequence. Two types of ED (ED-1 and ED-2) were attached to each of the 5′ query probes (see Materials and Methods), and we incorporated a mismatch base into the 5′ query probes at the fourth position from the SNP site to improve the precision of allele discrimination [20]. The 3′ query probe has a sequence complementary to the 3′-flanking region of the target SNP, and each of the probes has a D1 on its 3′ end. In the encoding step, the 5′ query and 3′ query probes are successfully concatenated by *Taq* DNA ligase, and the probes are fully complementary to adjacent regions on the target fragment [22]. The genotype is then converted into a type of ED and a type of D1. The types of ED and D1 designate the type of allele and SNP, respectively. After the encoding step, fluorescence is incorporated into the ligated products by asymmetric PCR using fluorescent-labeled primers (Cy3-ED-1 and Cy5-ED-2) and D1 primers. The D1 primers are a mixture of all D1s used in the assay. The Cy3- and Cy5-labeled PCR products are directly hybridized with the D1 probes on the DNA microarray to reveal SNP genotypes by reading signals from the various D1s. If the genomic DNA sample is homozygous for a certain SNP, a single color signal from Cy3 or Cy5 is detected from the corresponding spot on the DNA microarray. In contrast, both signals are present when the genomic DNA sample is heterozygous.

SNP selection and probe design

In a previous report, we investigated the ligation conditions in the encoding step using an SNP located in the *PLOD* gene on human chromosome 1p36 as a model SNP (JSNP ID IMS-JST068774) and determined the parameters for 5′ query and 3′ query probes [20]. We then randomly selected 96 SNPs from a 610-kb region, including the *IL-4* and *IL-13* genes on human chromosome 5q31-33, which contains various candidate genes related to immune and allergic disorders. We subsequently designed probes for the 96 SNP sites to have a uniform melting temperature as that of *PLOD* SNP so as to give similar ligation efficiency among the 96 SNP sites to be analyzed in a single tube. We also incorporated a mismatch base into the 5′ query probe at the fourth position from the SNP site for all target SNPs. The 20-mer mismatch-induced 5′ query probes and 3′ query probes (average length) had melting temperatures of 50.7 ± 2.1 °C and 52.4 ± 1.5 °C, respectively. Here we found that the length of the 3′ query probe influences the ligation efficiency in the encoding step; when a longer 3′ query probe was used in the encoding step, stronger signal intensities were acquired on microarray detection (data not shown). Therefore, we used the lengthened 3′ query probes to 30-mer, and the average melting temperature of the lengthened 3′ query probes was 66.1 ± 3.5 °C. The sequence information for 5′ query probes and lengthened 3′ query probes is listed in Supplementary Table 3.

Optimization of reaction conditions

When we used the mismatch-induced 5′ query probes, indistinct clusters were observed from 5 SNPs (SNP 7, SNP 9, SNP 18, SNP 49, and SNP 93) (Fig. 2A). However, these 5 SNPs can be discriminatively genotyped with perfect

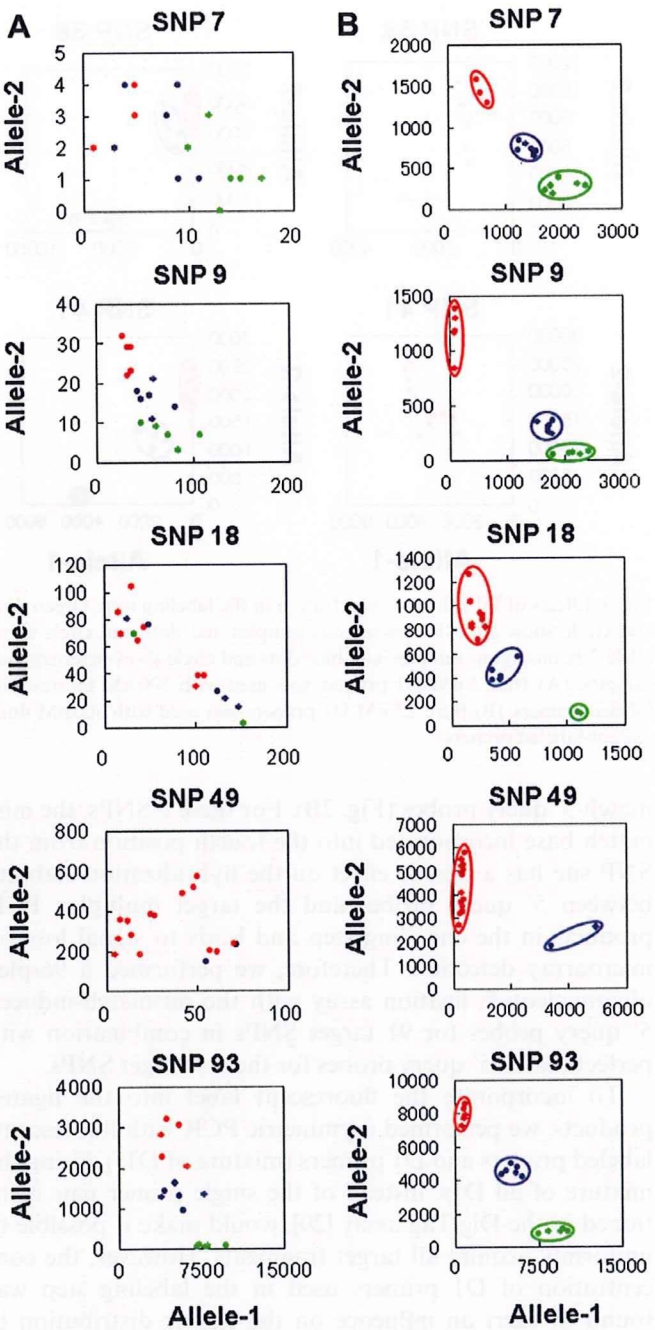

Fig. 2. Treatment of 5 failed SNPs with mismatch-induced 5′ query probes. Green dots and circle show allele-1 homozygous samples, red dots and circle show allele-2 homozygous samples, and blue dots and circle show heterozygous samples. (A) Mismatch-induced 5′ query probes, which have a mismatched base incorporated into the fourth position from the SNP base, were used. (B) Here 5′ query probes, which have a perfect match sequence for the target SNP, were used instead of mismatch-induced 5′ query probes.

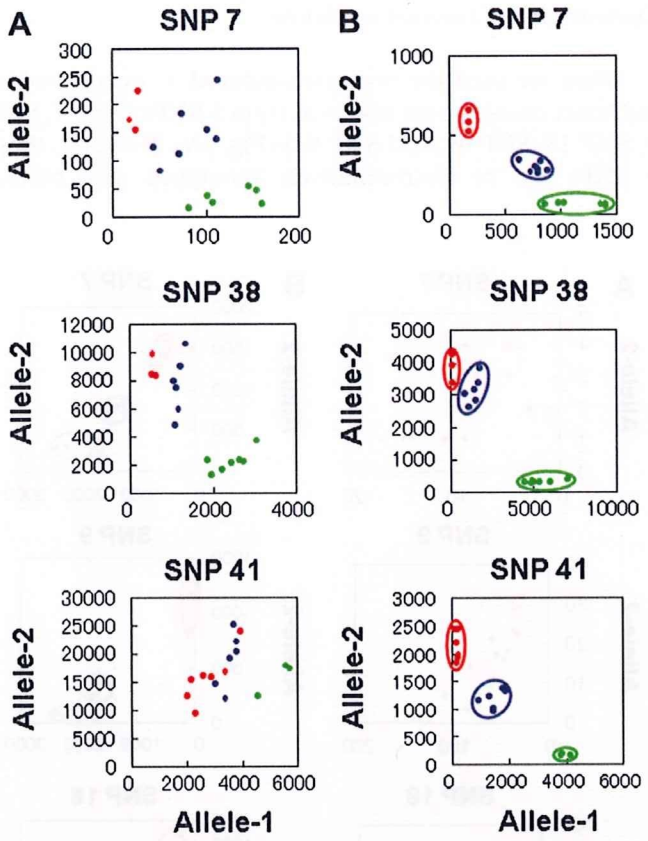

Fig. 3. Effects of D1 primer concentration in the labeling step. Green dots and circle show allele-1 homozygous samples, red dots and circle show allele-2 homozygous samples, and blue dots and circle show heterozygous samples. (A) Here 5 nM D1 primers was used with 500 nM fluorescent-labeled primers. (B) Here 2.5 nM D1 primers was used with 500 nM fluorescent-labeled primers.

match 5′ query probes (Fig. 2B). For these 5 SNPs, the mismatch base incorporated into the fourth position from the SNP site has a drastic effect on the hybridization stability between 5′ query probes and the target multiplex PCR products in the encoding step and leads to signal loss on microarray detection. Therefore, we performed a 96-plex oligonucleotide ligation assay with the mismatch-induced 5′ query probes for 91 target SNPs in combination with perfect match 5′ query probes for these 5 target SNPs.

To incorporate the fluorescent label into the ligated products, we performed asymmetric PCR with fluorescent-labeled primers and D1 primers (mixture of D1s). Using the mixture of all D1s, instead of the single primer pair mentioned in the DigiTag assay [20], would make it possible to uniformly acquire all target fragments. However, the concentration of D1 primers used in the labeling step was found to exert an influence on the cluster distribution in scatter diagrams. When we used 5 nM D1 primers with 500 nM fluorescent-labeled primers, dispersed and/or indiscrete clusters were observed for several SNPs (Fig. 3A). However, the dispersed and/or indiscrete clusters became convergent and/or discrete clusters when we used 2.5 nM D1 primers with 500 nM fluorescent-labeled primers (Fig. 3B). The D1 primers share the fluorescent-labeled primers in the labeling step, and the ratio of each D1 primer to fluorescent-labeled primer was approximately 1:2 at 2.5 nM and 1:1 at 5 nM. When the amount of each D1 primer was greater than the amount of fluorescent-labeled primer, strong false-positive signals were observed on microarray detection, leading to indiscrete clusters on scatter diagrams (data not shown). On the other hand, when the amount of each D1 primer was less than the amount of fluorescent-labeled primer, insufficient amplification occurred in a number of target SNPs, leading to weak signal intensities on microarray detection (data not shown). We found that the optimal ratio of D1 primer to fluorescent-labeled primer is approximately 1:2, irrespective of the multiplicity of the assay (number of SNPs to be analyzed).

Genotyping results

Multiplex PCR products, including the 96 SNP sites, showed similar band patterns as 48 individual DNA samples, although it was difficult to clearly discern all 96 PCR products due to limitations in electrophoretic resolution (Fig. 4A). We then performed a multiplexed oligonucleotide ligation assay using the multiplex PCR products as targets. To incorporate the fluorescent label into the ligated products, asymmetric PCR was performed using the fluorescent-labeled and D1 primers. DNA microarray revealed hybridization images of 24 individual samples from each of the 24 separated areas having 100 spots (96 probes for 96 SNPs and 4 probes for validation controls) (Fig. 4B). The hybridization image was analyzed using a DNA chip scanner, and the Cy3 and Cy5 signal intensities of each spot were plotted to produce a scatter diagram. The SNP genotypes of 16 genomic DNA samples, randomly selected from the 48 samples, were alternatively determined by direct sequencing and were used as reference data.

As a result of 96-plex genotyping under optimal labeling conditions using the mismatch-induced 5′ query probes in combination with the perfect match 5′ query probes for 5 SNPs, three distinct clusters corresponding to two homozygous genotypes and one heterozygous genotype were observed from 84 SNPs (exceptions were SNP 31, SNP 37, SNP 60, SNP 61, and SNP 87) (Fig. 4C). The remaining 7 SNPs (SNP 12, SNP 22, SNP 27, SNP 33, SNP 67, SNP 88, and SNP 91) were found to be monomorphic in 48 genomic DNA samples and were excluded from further analysis. For SNP 37, SNP 60, and SNP 87, drastically attenuated signal intensities were observed on microarray detection (Fig. 4D). Signal loss was caused by insufficient amplification of the target fragments on multiplex PCR because no amplified products were observed on singleplex PCR, even when the second candidate primer pairs were used. There were some structural obstacles in the target region, although we could not identify any characteristic structures. SNP 31 and SNP 61 were found to have strong false-positive signals, leading to indistinct clusters on scatter diagrams (Fig. 4E). The false-positive signals would be caused by the misligation in the encoding step that was

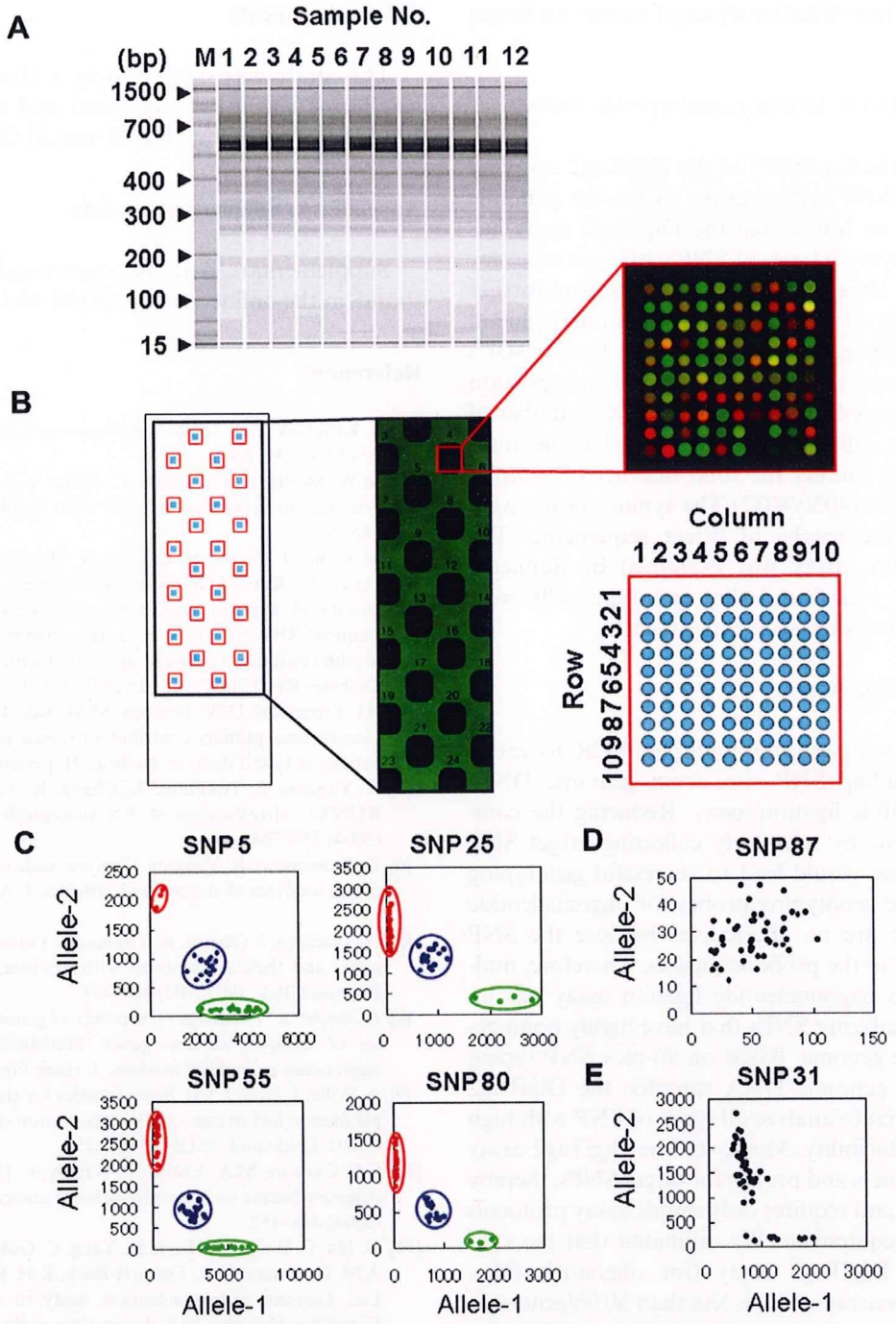

Fig. 4. Multiplex SNP typing for 96 SNPs using 48 individual genomic DNA samples. (A) Gel images of multiplex PCR products with different samples. In all sample lanes, sample bands were observed between two inner markers: 15 and 1500 bp. (B) Hybridization images of DNA microarray. (C) Scatter plot diagrams for 4 randomly selected SNPs from 84 working SNPs. Green dots and circle show allele-1 homozygous samples, red dots and circle show allele-2 homozygous samples, and blue dots and circle show heterozygous samples. (D) Example of the typing-failed SNP caused by insufficient amplification of target fragment in multiplex PCR. (E) Example of the typing-failed SNP that was found to have strong false-positive signals.

reported to be prone to occur when the mismatched pairs are G–T, G–A, G–G, A–G, and T–G [23,24]. Of the 2 misligated SNPs, 1 had an A–G mismatch (SNP 31) and the other had a T–G mismatch (SNP 61) between the 5′ query probe and the target fragment. These 2 SNPs were undetectable, even when 5′ query probes with the mismatched base incorporated into different positions were used (data not shown). Although there were other G–T, G–A, G–G, A–G, and T–G mismatches within the set of 84 working SNPs, we consider that these mismatches would increase the likelihood of misligation in some cases. In the future, we will be able to search for the cause of misligation by

accumulating data from failed analyses of numerous target SNPs.

Conversion rate, call rate, accuracy, and reproducibility

We investigated the feasibility of the DigiTag2 assay by performing 96-plex SNP typing using 48 human genomic DNA samples, and we found that the DigiTag2 assay has the potential to analyze all types of SNP with high accuracy and reproducibility. Here we excluded 7 SNPs from further analysis because they were revealed to be monomorphic in 48 samples. The DigiTag2 assay was found to have a 94.4% (84/89) conversion rate, which is defined as the proportion of successfully genotyped SNPs among the total number of SNPs examined. The call rate, which is defined as the number of genotype calls among the total number of samples examined, was 99.95% (4030/4032) The typing results were 100% identical to the results of direct sequencing. The reproducibility of this assay was examined by duplicate experiments, and it was found that genotype calls were 100% identical between duplicate experiments.

Advantages of DigiTag2 assay

The DigiTag2 assay performs multiplex PCR to excise target regions, including SNP sites from genomic DNA, prior to oligonucleotide ligation assay. Reducing the complexity of the genome by selectively collecting target SNP sites from the genome would lead to successful genotyping [25]. In designing the genotyping probes for oligonucleotide ligation assay, there are no alternatives because the SNP sequence is included in the probe sequences. Therefore, multiplex PCR prior to oligonucleotide ligation assay has an important role in analyzing SNPs that have highly homogeneous regions in the genome. Based on 96-plex SNP typing using 48 individual genomic DNA samples, the DigiTag2 assay has the potential to analyze all types of SNP with high accuracy and reproducibility. Moreover, the DigiTag2 assay uses unmodified primers and probes for target SNPs, thereby reducing assay cost, and requires only simple assay protocols without specialized equipment. We estimated that the running cost for the DigiTag2 assay (for oligonucleotides, reagents, DNA microarrays, etc.) is less than $0.06/genotype. The DigiTag2 assay can use the same set of D1s and EDs for any set of target SNPs, thereby enabling 96-plex genotyping with the same assay protocols and the same microarray having the same set of probes. However, hybridization products, which are prepared in the labeling step, may cross-hybridize to the wrong D1 probes on DNA microarray due to SNP-specific sequences being introduced into the hybridization products. With regard to the 96 target SNPs selected in this study, there is no evidence of cross-hybridization between D1 probes and SNP-specific sequences. Cross-hybridization may be avoided by predicting the interaction between D1 probes and SNP-specific sequences. In the future, we will attempt to predict cross-hybridization by accumulating data from failed analyses of numerous target SNPs.

Acknowledgments

This study was supported by a Grant-in-Aid for Scientific Research on Priority Areas and the New Energy and Industrial Technology Development Organization.

Appendix A. Supplementary data

Supplementary data associated with this article can be found, in the online version, at doi:10.1016/j.ab.2007.02.005.

References

[1] L. Kruglyak, D.A. Nickerson, Variation is the spice of life, Nat. Genet. 27 (2001) 234–236.
[2] M.W. McBride, D. Graham, C. Delles, A.F. Dominiczak, Functional genomics in hypertension, Curr. Opin. Nephrol. Hypertens. 15 (2006) 145–151.
[3] M. Ochi, H. Osawa, H. Onuma, A. Murakami, T. Nishimiya, F. Shimada, K. Kato, I. Shimizu, K. Shishino, M. Murase, Y. Fujii, J. Ohashi, H. Makino, The absence of evidence for major effects of the frequent SNP +299 G > A in the resistin gene on susceptibility to insulin resistance syndrome associated with Japanese type 2 diabetes, Diabetes Res. Clin. Pract. 61 (2003) 191–198.
[4] B.I. Freedman, D.W. Bowden, M.M. Sale, C.D. Langefeld, S.S. Rich, Genetic susceptibility contributes to renal and cardiovascular complications of type 2 diabetes mellitus, Hypertension 48 (2006) 8–13.
[5] R. Yamada, S. Tokuhiro, X. Chang, K. Yamamoto, SLC22A4 and RUNX1: identification of RA susceptible genes, J. Mol. Med. 82 (2004) 558–564.
[6] K. Yamamoto, R. Yamada, Genome-wide single nucleotide polymorphism analyses of rheumatoid arthritis, J. Autoimmun. 25 (2005) 12–15.
[7] N. Tsuchiya, J. Ohashi, K. Tokunaga, Variations in immune response genes and their associations with multifactorial immune disorders, Immunol. Rev. 190 (2002) 169–181.
[8] J. Ohashi, K. Tokunaga, The power of genome-wide association studies of complex disease genes: Statistical limitations of indirect approaches using SNP markers, J. Hum. Genet. 46 (2001) 478–482.
[9] A. Wille, J. Hoh, J. Ott, Sum statistics for the joint detection of multiple disease loci in case-control association studies with SNP markers, Genet. Epidemiol. 25 (2003) 350–359.
[10] C.S. Carlson, M.A. Eberle, L. Kruglyak, D.A. Nickerson, Mapping complex disease loci in whole-genome association studies, Nature 429 (2004) 446–452.
[11] N. Hu, C. Wang, Y. Hu, H.H. Yang, C. Giffen, Z-Z. Tang, X-Y. Han, A.M. Goldstein, M.R. Emmert-Buck, K.H. Buetow, P.R. Taylor, M.P. Lee, Genome-wide association study in esophageal cancer using GeneChip Mapping 10 K Array, Cancer Res. 65 (2005) 2542–2546.
[12] D.J. Schaid, J.C. Guenther, G.B. Christensen, S. Hebbring, C. Rosenow, C.A. Hilker, S.K. McDonnell, J.M. Cunningham, S.L. Slager, M.L. Blute, S.N. Thibodeau, Comparison of microsatellites versus single-nucleotide polymorphisms in a genome linkage screen for prostate cancer-susceptibility loci, Am. J. Hum. Genet. 75 (2004) 948–965.
[13] T. Arinami, T. Ohtsuki, H. Ishiguro, H. Ujike, Y. Tanaka, Y. Morita, M. Mineta, M. Takeichi, S. Yamada, A. Imamura, K. Ohara, H. Shibuya, K. Ohara, Y. Suzuki, T. Muratake, N. Kaneko, T. Someya, T. Inada, T. Yoshikawa, T. Toyota, K. Yamada, T. Kojima, S. Takahashi, O. Osamu, T. Shinkai, M. Nakamura, H. Fukuzako, T. Hashiguchi, S. Niwa, T. Ueno, H. Tachikawa, T. Hori, T. Asada, S. Nanko, H. Kunugi, R. Hashimoto, N. Ozaki, N. Iwata, M. Harano, H. Arai, T. Ohnuma, I. Kusumi, T. Koyama, H. Yoneda, Y. Fukumaki, H. Shibata, S. Kaneko, H. Higuchi, N. Yasui-Furukori, Y. Numachi, M. Itokawa, Y. Okazaki, Japanese Schizophrenia Sib-Pair Linkage

Group, Genome-wide high-density SNP linkage analysis of 236 Japanese families supports the existence of schizophrenia susceptibility loci on chromosomes 1p, 14q, and 20p, Am. J. Hum. Genet. 77 (2005) 937–944.

[14] P.M. Holland, R.D. Abramson, R. Watson, D.H. Gelfand, Detection of specific polymerase chain reaction product by utilizing the 5′→3′ exonuclease activity of *Thermus aquaticus* DNA polymerase, Proc. Natl. Acad. Sci. USA 88 (1991) 7276–7280.

[15] N. Pourmand, E. Elahi, R.W. Davis, M. Ronaghi, Multiplex pyrosequencing, Nucleic Acids Res. 30 (2002) e31.

[16] K. Lindroos, U. Liljedahl, M. Raitio, A-C. Syvänen, Minisequencing on oligonucleotide microarrays: Comparison of immobilisation chemistries, Nucleic Acids Res. 29 (2001) e69.

[17] J. Tost, I.G. Gut, Genotyping single nucleotide polymorphisms by mass spectrometry, Mass Spectrom. Rev. 21 (2002) 388–418.

[18] M.S. Bray, E. Boerwinkle, P.A. Doris, High-throughput multiplex SNP genotyping with MALDI–TOF mass spectrometry: Practice, problems, and promise, Hum. Mutat. 17 (2001) 296–304.

[19] A.R. Tobler, S. Short, M.R. Andersen, T.M. Paner, J.C. Briggs, S.M. Lambert, P.P. Wu, Y. Wang, A.Y. Spoonde, R.T. Koehler, N. Peyret, C. Chen, A.J. Broomer, D.A. Ridzon, H. Zhou, B.S. Hoo, K.C. Hayashibara, L.N. Leong, C.N. Ma, B.B. Rosenblum, J.P. Day, J.S. Ziegle, F.M. De La Vega, M.D. Rhodes, K.M. Hennessy, H.M. Wenz, The SNPlex genotyping system: A flexible and scalable platform for SNP genotyping, J. Biomol. Tech. 16 (2005) 396–404.

[20] N. Nishida, T. Tanabe, K. Hashido, K. Hirayasu, M. Takasu, A. Suyama, K. Tokunaga, DigiTag assay for multiplex single nucleotide polymorphism typing with high success rate, Anal Biochem. 346 (2005) 281–288.

[21] H. Yoshida, A. Suyama, Solution to 3-SAT by breadth first search, DIMACS Ser. Discrete Math. Theor. Comput. Sci. 54 (2000) 9–22.

[22] F. Barany, Genetic disease detection and DNA amplification using cloned thermostable ligase, Proc. Natl. Acad Sci. USA 88 (1991) 189–193.

[23] J.N. Housby, E.M. Southern, Fidelity of DNA ligation: A novel experimental approach based on the polymerisation of libraries of oligonucleotides, Nucleic Acids Res. 26 (1998) 4259–4266.

[24] J. Luo, D.E. Bergstrom, F. Barany, Improving the fidelity of *Thermus thermophilus* DNA ligase, Nucleic Acids Res. 24 (1996) 3071–3078.

[25] H. Matsuzaki, H. Loi, S. Dong, Y-Y. Tsai, J. Fang, J. Law, X. Di, W-M. Liu, G. Yang, G. Liu, J. Huang, G.C. Kennedy, T.B. Ryder, G.A. Marcus, P.S. Walsh, M.D. Shriver, J.M. Puck, K.W. Jones, R. Mei, Parallel genotyping of over 10,000 SNPs using a one-primer assay on a high-density oligonucleotide array, Genome Res. 14 (2004) 414–425.

American Journal of Gastroenterology
© 2007 by Am. Coll. of Gastroenterology
Published by Blackwell Publishing

ISSN 0002-9270
doi: 10.1111/j.1572-0241.2006.01038.x

Clearance of HCV Improves Insulin Resistance, Beta-Cell Function, and Hepatic Expression of Insulin Receptor Substrate 1 and 2

Takumi Kawaguchi, M.D., Ph.D.,[1,2] Tatsuya Ide, M.D., Ph.D.,[1,2] Eitaro Taniguchi, M.D., Ph.D.,[2] Eiichi Hirano, Ph.D.,[1] Minoru Itou, M.D.,[2] Shuji Sumie, M.D.,[2] Yumiko Nagao, M.D., DDS.,[1,2] Chikatoshi Yanagimoto, M.D.,[2] Shinichiro Hanada, M.D., Ph.D.,[2] Hironori Koga, M.D.,[2] and Michio Sata, M.D.[1,2]

[1]*Department of Digestive Disease Information and Research,* [2]*Division of Gastroenterology, Department of Medicine, Kurume University School of Medicine, Kurume, Japan*

OBJECTIVES: **Hepatitis C virus (HCV) infection is linked to greater insulin resistance. Although HCV itself is a candidate for the development of insulin resistance, the effects of antiviral treatment on impaired glucose metabolism remain unclear. The aim of this study is to examine the effects of clearance of HCV on insulin resistance, beta-cell function, and hepatic expression of insulin receptor substrate (IRS)1/2, central molecules for insulin signaling.**

METHODS: **We analyzed 89 biopsy-proven patients with chronic HCV infection. Patients received interferon-α or interferon-α plus ribavirin for 6 months and were classified into three groups at 6 months after the conclusion of antiviral therapy according to their response to antiviral therapy: sustained responders (N = 29), relapsers (N = 12), and nonresponders (N = 48). Insulin resistance and beta-cell function were assessed by the homeostasis model assessment method (HOMA-IR and HOMA-%B, respectively). Hepatic expression of IRS1/2 was evaluated by immunoblotting and immunostaining in 14 sustained responders.**

RESULTS: **In nonresponders and relapsers, there were no significant changes in HOMA-IR and HOMA-%B values after antiviral therapy. On the other hand, in sustained responders, HOMA-IR values significantly decreased to 1.7 ± 0.8 from 3.1 ± 1.1 ($P < 0.05$) after antiviral therapy. Similarly, HOMA-%B values significantly decreased to 90.6 ± 10.0 from 113.7 ± 15.3 ($P < 0.05$). Immunoblotting showed a threefold increase in IRS1/2 expression after clearance of HCV. Immunostaining revealed that greater IRS1/2 expression was seen in hepatocytes.**

CONCLUSIONS: **We showed that clearance of HCV improves insulin resistance, beta-cell function, and hepatic IRS1/2 expression.**

(Am J Gastroenterol 2007;102:1–7)

INTRODUCTION

Chronic hepatitis C virus (HCV) infection is associated with a greater risk for the development of insulin resistance (1). Greater insulin resistance is more prevalent among patients with HCV infection compared with those with other liver diseases and with the general population (2). In patients with HCV infection, insulin resistance is involved in progression of hepatic fibrosis (3), the development of hepatocellular carcinoma (4, 5), extrahepatic manifestations (6), and prognosis (7). Thus, insulin resistance plays a crucial role in patients with HCV infection.

Insulin resistance can be caused by many factors. In general, obesity, inflammation, and various kinds of metabolic disorders are common factors for the development of insulin resistance. Similarly, body mass index (BMI), serum tumor necrosis factor-α (TNF-α) and hepatic iron concentrations, and hepatic steatosis are reported to be possible causative factors for the development of insulin resistance in patients with HCV infection (8–11). In addition to these factors, HCV itself is also known to have a variety of biological effects (12).

In HCV core transgenic mice, the development of insulin resistance is seen by 1 month of age, in the absence of either overt liver injury or excessive body weight gain (12, 13). Furthermore, even if liver function is restored by transplantation, postliver transplantation diabetes mellitus occurs more frequently among patients who undergo transplantation for HCV than for other conditions (14). Although precise mechanisms for HCV-associated insulin resistance have not been fully elucidated, we recently demonstrated the involvement of insulin receptor substrate 1 and 2 (IRS1/2), central molecules in insulin signaling. Downregulation of IRS1/2 is seen in

livers from HCV core transgenic mice as well as in patients with HCV infection (15). Thus, HCV itself is a candidate risk factor for the development of insulin resistance.

If HCV is a causal factor, then clearance of HCV might decrease insulin resistance just as histologic improvement of fibrosis and reduction in the risk of hepatocellular carcinoma are seen in patients with hepatitis C who have sustained response to interferon therapy (16, 17). The ability of antiviral therapy to improve glucose metabolism would support the notion that HCV causes insulin resistance in patients with HCV infection. Accordingly, we studied the effects of HCV clearance on insulin resistance, beta-cell function, and hepatic expression of IRS1/2.

MATERIALS AND METHODS

Materials

All reagents were purchased from Wako Pure Chemical Industries (Osaka, Japan) unless otherwise indicated.

Patients

We analyzed 89 patients with HCV infection. The diagnosis was based on elevated serum aminotransferase level, histological examination, consistent detection of anti-HCV, and HCV-RNA. Patients who coincided with other causes of liver disease such as chronic hepatitis B, autoimmune hepatitis, or alcoholic liver disease (greater than 80 g alcohol per day for at least 1-month duration prior to the onset of illness) were excluded, as were those who had been taking corticosteroids or those with a history of, or evidence of, pancreatitis or a pancreatic tumor. Clinical data collected before antiviral therapy included age, sex, and alcohol use. BMI was calculated as body weight in kilograms divided by the square of height in meters (kg/m^2). Informed consent for participation in the study was obtained from each subject. The study protocol conformed to the ethical guidelines of the 1975 Declaration of Helsinki as reflected in prior approval by the Ethics Committee of the Kurume University School of Medicine. None of the subjects was institutionalized.

Laboratory Determinations

Venous blood samples were taken in the morning after a 12-h overnight fast. Plasma glucose, serum aspartate aminotransferase, alanine aminotransferase, albumin, total bilirubin, and immunoreactive insulin (IRI) levels were measured by using standard clinical methods (Department of Clinical Laboratory, Kurume University Hospital). Beta-cell function and insulin resistance were calculated on the basis of fasting levels of plasma glucose and IRI, according to the homeostasis model assessment (HOMA) method (18). The formulas for the HOMA model are as follows: beta-cell function (HOMA-%B) = fasting IRI (μU/mL) × 360/(fasting glucose (mg/dL) − 63); insulin resistance (HOMA-IR) = fasting glucose (mg/dL) × fasting IRI (μU/mL)/405. HCV genotyping was performed according to Okamoto's method (19) and genotypes were classified according to Simmonds's classification system (20). An Amplicor-HCV-Monitor 1.0 (Roche Diagnostics K.K., Tokyo, Japan) was used to quantify HCV-RNA levels.

Liver Biopsy

Liver tissue was obtained by percutaneous ultrasound image-guided liver biopsy. The biopsies were performed by two staff gastroenterologists using a Pro-Mag™ Biopsy Needle (Medical Device Technologies Inc., Gainesville, FL), which has a biopsy specimen notch of 20.00 mm in width and 2.05 mm in diameter. More than 95% (vol/vol) of liver tissue was used for histological and immunostaining analyses. Less than 5% (vol/vol) of liver tissue was homogenized and 80 μg of protein was used for immunoblotting analysis.

Histological Data

For each patient, a liver biopsy specimen was fixed in 10% formalin buffer and stained with hematoxylin-eosin. Liver biopsy specimens were evaluated by a single, experienced pathologist who was unaware of the patients' clinical and laboratory data. The specimens were scored according to the METAVIR scoring system (21), which is suited for evaluation of chronic hepatitis C.

Treatment Outcome

All patients were treated with 3 to 10 million U of interferon-α (interferon-α2a, Nippon Roche K.K., Tokyo, Japan; interferon-α2b, Schering-Plough K.K., Osaka, Japan; or natural interferon-α, Dainippon Sumitomo Pharma Co., Osaka, Japan) by subcutaneous injection three times per week, or 6 to 10 million U of interferon-α2b plus ribavirin (600 to 1,000 mg daily, Schering-Plough Co) for 6 months. Patients were followed up until 6 months after the conclusion of antiviral therapy and classified into three groups: sustained responders (N = 29), who had undetectable serum HCV-RNA; relapsers (N = 12), who had undetectable HCV-RNA at the end of antiviral therapy but HCV-RNA relapse during follow-up; and nonresponders (N = 48), who had detectable HCV-RNA during and after treatment.

Immunoblotting

Liver tissue was homogenized on ice in 1 mmol/L $NaHCO_3$ containing protease inhibitors, stored at −80°C as previously described (22, 23). Equal amounts of protein (40 μg) from liver homogenates were subjected to sodium dodecyl sulfate-polyacrylamide gel electrophoresis on a 7.5% acrylamide gel. The resolved proteins were transferred electrophoretically onto polyvinylidene difluoride membranes (Amersham International, Buckinghamshire, UK). The membranes were incubated with an antihuman IRS1 polyclonal antibody (Santa Cruz Biotechnology, Santa Cruz, CA) or an antihuman IRS2 polyclonal antibody (Santa Cruz Biotechnology), and were subsequently incubated with an HRP-conjugated goat antirabbit IgG (Amersham International). The membranes were then incubated with chemiluminescence reagents (ECL kit, Amersham International) and immediately exposed on

radiograph film. Immunoblotting intensities were determined using NIH-Image J (developed at the National Institutes of Health and available from the Internet by an anonymous FTP from http://rsb.info.nih.gov/ij/download.html) as previously described (22, 23).

Immunohistochemistry

In 14 sustained responders, liver biopsy was performed before and after conclusion of antiviral therapy. Paraffin-embedded liver sections from patients with HCV infection were deparaffinized and subjected to immunohistochemical staining using a Vectastain ABC kit (Vector Laboratories, Burlingame, CA) with an antihuman IRS1 polyclonal antibody (Santa Cruz Biotechnology) or an antihuman IRS2 polyclonal antibody (Santa Cruz Biotechnology), and developed with 3,3′-diaminobenzidine (DAB). The primary antibodies for IRS1/2 were used at a 1:100 dilution. The specificity of IRS1/2 staining was confirmed by immunization using an excess amount of the N-terminal peptide of IRS1/2.

Statistical Analysis

All data are expressed as mean ± SD. The Wilcoxon's single-rank test was employed for analysis of paired samples. Statistical comparisons among multiple groups were performed by analysis of variance followed by Scheffe's *post hoc* test. P values < 0.05 were considered significant.

RESULTS

Characteristics of the Patients

Characteristics of the patients before antiviral therapy are summarized in Table 1. There was no significant difference in age or sex distribution among the groups. In sustained responders, higher infection rates of genotype 2 (62.0%) were seen compared with nonresponders (12.5%) or relapsers (16.7%). Although HCV viral load, hepatic fibrosis, and HOMA-IR were lower in sustained responders, BMI and hepatic necroinflammatory activity were not significantly different among the groups.

Changes in BMI, Insulin Resistance, and Beta-Cell Function After Antiviral Therapy

Changes in BMI, insulin resistance, and beta-cell function after antiviral therapy are summarized in Figure 1. In nonresponders (N = 48), BMI significantly decreased to 21.7 ± 1.6 kg/m^2 from 22.7 ± 2.3 kg/m^2 ($P < 0.01$) at the end of follow-up. However, there were no significant changes in HOMA-IR and HOMA-%B values at the end of follow-up compared with those before antiviral therapy (HOMA-IR 4.0 ± 1.7 *vs* 3.6 ± 1.2, $P = 0.11$, HOMA-%B 120.0 ± 26.1 *vs* 112.4 ± 24.1, $P = 0.09$) (Fig. 1A). In relapsers (N = 12) no significant differences were seen in BMI (21.8 ± 1.7 kg/m^2 *vs* 22.1 ± 1.6 kg/m^2, $P = 0.70$), HOMA-IR values (3.7 ± 1.2 *vs* 3.6 ± 1.2, $P = 0.69$), and HOMA-%B values (121.5 ± 13.3 *vs* 117.4 ± 17.4, $P = 0.24$) at the end of follow-up compared with those before antiviral therapy (Fig. 1B). In sustained responders (N = 29), there was no significant difference in BMI at the end of follow-up (22.6 ± 1.6 kg/m^2 *vs* 21.9 ± 1.9 kg/m^2, $P = 0.07$). On the other hand, HOMA-IR values significantly decreased to 2.2 ± 0.7 from 3.1 ± 1.0 ($P < 0.01$) by the end of follow-up. Similarly, HOMA-%B values significantly decreased to 92.6 ± 14.0 from 113.7 ± 21.3 ($P < 0.01$) (Fig. 1C).

Changes in Hepatic Expression of IRS1/2 in Sustained Responders

Immunoblotting demonstrated a significant increase in expression of IRS1/2 after antiviral therapy in livers from sustained responders (Fig. 2A). After antiviral therapy, mean IRS1 and IRS2 intensities showed a two- and threefold increase, respectively, compared with intensities before antiviral therapy (Table 2). In immunostaining, IRS1 occurred mainly in lymphocytes (Fig. 2B, left upper panel) before antiviral therapy, but occurred in hepatocytes after antiviral therapy (Fig. 2B, right upper panel). On the other hand, IRS2

Table 1. Characteristics of the Patients

	Nonresponders	Relapsers	Sustained Responders	*P* Value
N	48	12	29	
Age (yr)	61.7 ± 7.7	63.2 ± 6.1	58.5 ± 8.6	N.S.
Male/female	27/21	8/4	19/10	N.S.
BMI	22.7 ± 2.3	21.9 ± 1.7	22.6 ± 1.6	N.S.
Aspartate aminotransferase (U/L)	68.1 ± 36.3	75.7 ± 24.4	64.2 ± 30.4	N.S.
Alanine aminotransferase (U/L)	92.5 ± 35.1	86.3 ± 24.8	88.7 ± 30.4	N.S.
γ-glutamyltranspeptidase (U/L)	97.9 ± 44.6	88.0 ± 37.1	94.0 ± 34.9	N.S.
Total bilirubin (mg/dL)	0.84 ± 0.11	0.81 ± 0.20	0.85 ± 0.15	N.S.
Albumin (g/dL)	3.79 ± 0.26	3.71 ± 0.29	3.87 ± 0.28	N.S.
Genotype 1/2	42/6	10/2	11/18	0.008
Viral load (× 10^3 copies)	485 ± 299	534 ± 254	309 ± 212	0.024
Necroinflammatory activity	2.04 ± 0.71	2.00 ± 0.74	1.90 ± 0.78	N.S.
Fibrosis	2.29 ± 0.74	2.25 ± 0.87	1.82 ± 0.81	0.046
HOMA-IR	3.95 ± 1.69	3.73 ± 1.21	3.07 ± 0.95	0.01

Data are expressed as mean ± SD or as number of patients.
BMI = body mass index; HOMA-IR = homeostasis model assessment for insulin resistance.

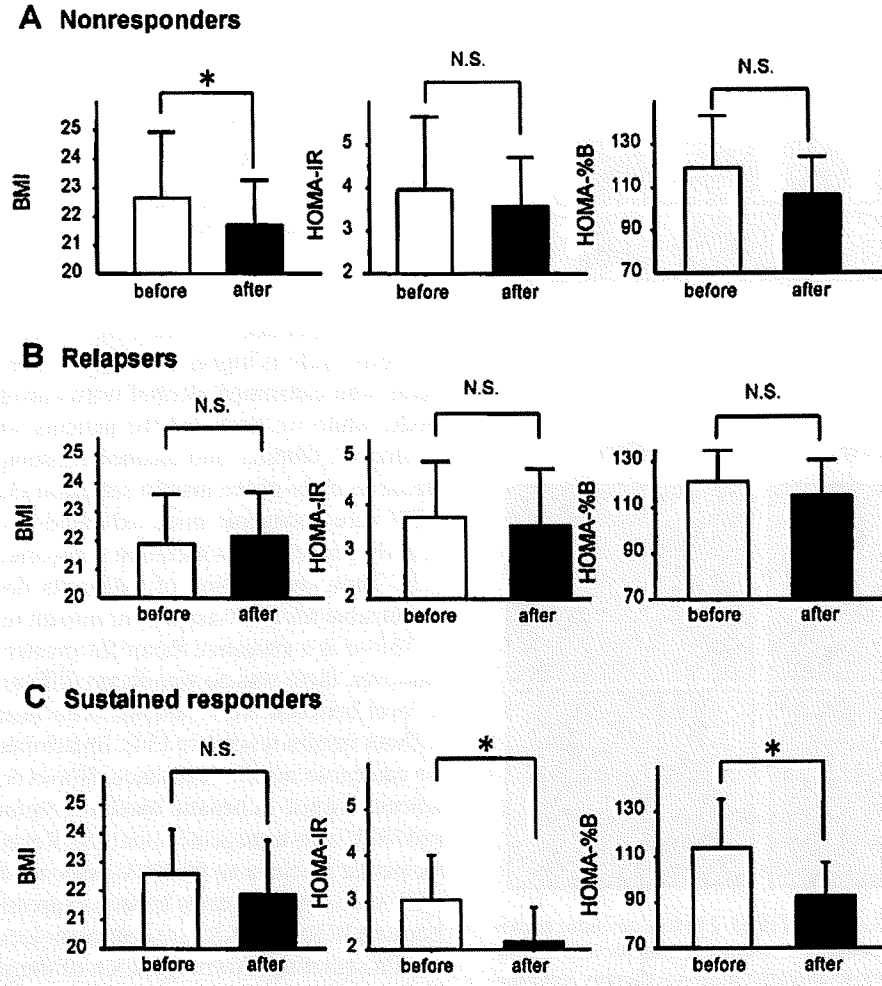

Figure 1. BMI, HOMA-IR, and HOMA-%B before and after antiviral therapy in nonresponders (N = 48; *A*), relapsers (N = 12; *B*), and sustained responders (N = 29; *C*). Data were obtained before antiviral therapy and 6 months after its conclusion. Data are expressed as mean ± SD. $^{*}P < 0.01$. N.S., not significant.

occurred in hepatocytes both before and after antiviral therapy (Fig. 2B, lower panels). After antiviral therapy, expression of IRS2 was upregulated mainly in periportal hepatocytes (Fig. 2B, right lower panel).

DISCUSSION

The present study demonstrates that clearance of HCV improves HOMA-IR, HOMA-%B, and hepatic expression of IRS1/2. These findings indicate that HCV itself is involved in the development of insulin resistance.

Insulin resistance can be caused by many factors. Obesity is a common factor for the development of insulin resistance (24). Although greater insulin resistance was seen in patients with chronic hepatitis C, BMI values were within normal limits in this study. Improved HOMA-IR was only seen in sustained responders and HOMA-IR remained unchanged in nonresponders, despite a decrease in BMI after antiviral therapy. In an epidemiologic study, Bahtiyar *et al.* reported that obesity is not associated with the development of insulin resistance in patients with HCV infection (25). In addition, the development of insulin resistance is seen by 1 month of age, in the absence of either overt liver injury or excessive body weight gain in HCV core transgenic mice (13) and serum HCV core protein levels are associated with HOMA-IR values in patients with chronic hepatitis C (15). Moreover, a significant increase in the incidence of diabetes was seen in subjects with high titers of HCV core compared with subjects with low titers of HCV core or anti-HCV-negative subjects at the population level during 7 yr of follow-up (26). Taken together, these findings suggest that HCV itself causes insulin resistance.

Interferon is known to induce insulin resistance. However, our results showed that interferon leads to a reduction in insulin resistance in sustained responders. Even in nonresponders or relapsers, interferon did not worsen insulin resistance. Interferon-induced insulin resistance is observed only in the early phase of treatment (27). Indeed, after 3 months of treatment, interferon-induced insulin resistance disappears (28).

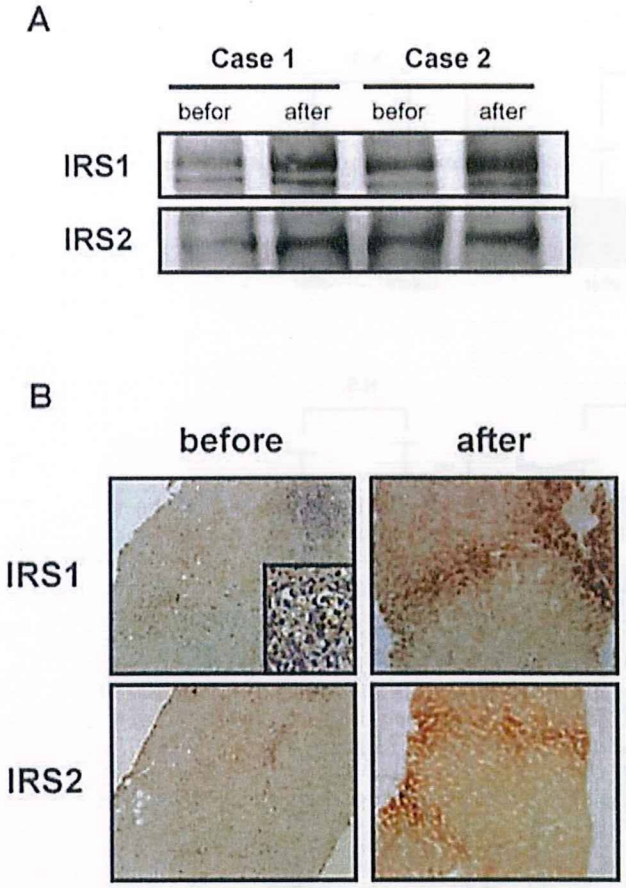

Figure 2. Protein expression levels of IRS1/2 before and after antiviral therapy in sustained responders. Immunoblotting for IRS1/2 (*A*). Proteins in liver extracts before and after antiviral therapy were immunoblotted with anti-IRS1 antibodies (upper panel) or anti-IRS2 antibodies (lower panel). Immunostaining for IRS1/2 (*B*). Liver sections before and after antiviral therapy were immunostained with anti-IRS1 antibodies (upper panels) or anti-IRS2 antibodies (lower panels). Expression of IRS1 and IRS2 were visualized by 3,3′-diaminobenzidine (brown). Expression of IRS1 in lymphocytes was shown. Original magnification ×400. Protein expression levels of IRS1/2 were examined in 14 sustained responders and representative immunoblotting and immunostaining images are shown.

Romero-Gomez *et al.* reported that improved insulin resistance during and after interferon therapy is correlated with a positive response to antiviral therapy (29), which is in good agreement with our findings. These finding also suggest the involvement of HCV in the development of insulin resistance.

Pancreatic beta-cells play a crucial role in maintaining glucose homeostasis. Although HCV infects not only liver but also pancreas (30), our results demonstrated that beta-cell function, especially the ability to secrete insulin, was preserved in patients with chronic hepatitis C. Because HOMA-%B was significantly decreased after antiviral therapy in sustained responders, increase in HOMA-%B seems to be an adaptation against greater insulin resistance. On the other hand, Narita *et al.* reported that beta-cell function is significantly decreased in patients with HCV infection (31). Although the reasons for this discrepancy are not clear, it could be explained by following reasons: First, BMI in the previous study is higher than that in our study. Second, patients who consumed alcohol were enrolled in the previous study, while we excluded the patients who had >80 g/day of alcohol. Obesity and alcohol consumption lead to a decrease in early-phase insulin secretion (32, 33). In addition, HCV core-transgenic mice exhibited a significant increase in early-phase insulin secretion compared with control mice (13). Thus, dysfunction of beta-cells does not seem to be responsible for HCV-associated insulin resistance.

Table 2. Hepatic Expression Levels of IRS1/2 Before and After Antiviral Therapy in Sustained Responders

	N	Before (Arbitrary Units)	After (Arbitrary Units)	*P*
IRS1	14	83.3 ± 47.9	156.8 ± 47.5	0.002
IRS2	14	31.7 ± 16.4	88.0 ± 33.8	0.001

Data are expressed as mean ± SD.

TNF-α is a causative factor for greater insulin resistance. However, there was no significant difference in serum TNF-α level between HCV patients with insulin resistance and without insulin resistance (34). Impairment of insulin receptor can cause insulin resistance. However, there was no significant change in hepatic insulin receptor between controls and HCV core-transgenic mice (15). Recently, we identified a molecular mechanism for HCV-associated insulin resistance. HCV core downregulates hepatic expression of IRS1/2 (15). Because IRS1 and IRS2 are central molecules in intracellular insulin signaling, downregulation of these molecules should decrease downstream insulin effects such as glucose uptake, thereby contributing to insulin resistance. In this study, we first demonstrated increases in hepatic expression of IRS1/2 after antiviral therapy in sustained responders. These findings support our proposed molecular mechanism that HCV directly downregulates hepatic expression of IRS1/2.

In conclusion, we showed that clearance of HCV improves HOMA-IR, HOMA-%B, and hepatic expression of IRS1/2. These findings indicate that HCV itself is involved in the development of insulin resistance in patients with HCV infection.

ACKNOWLEDGMENTS

The authors thank Yumi Ogo and Mari Hagihara for technical assistance. This study was supported, in part, by a Grant-in-Aid for Scientific Research (C) (No. 16590648 to M.S.) from the Ministry of Education, Culture, Sports, Science, and Technology of Japan, the Vehicle Racing Commemorative Foundation, and the 21st Century COE Program for Medical Science, Kurume University. A part of this study was presented at the 54th Annual Meeting of the American Association for the Study of Liver Diseases (Boston, MA) in October 2005 and published in abstract form (Hepatology 2005:42:540A).

STUDY HIGHLIGHTS

What Is Current Knowledge

- Greater insulin resistance and hyperinsulinemia are seen in patients with hepatitis C virus (HCV) infection.
- Insulin receptor substrate 1 and 2 (IRS1/2), central molecules in insulin signaling, are downregulated in livers from patients with HCV infection.

What Is New Here

- Clearance of HCV reduced insulin resistance and improved hyperinsulinemia.
- Hepatic expression of IRS1/2 was increased by clearance of HCV.

Reprint requests and correspondence: Takumi Kawaguchi, M.D., Ph.D., Department of Digestive Disease Information and Research, Division of Gastroenterology, Department of Medicine, Kurume University School of Medicine, 67 Asahi-machi, Kurume 830-0011, Japan.

Received September 8, 2006; accepted October 20, 2006.

REFERENCES

1. Allison ME, Wreghitt T, Palmer CR, et al. Evidence for a link between hepatitis C virus infection and diabetes mellitus in a cirrhotic population. J Hepatol 1994;21:1135–9.
2. Mason AL, Lau JY, Hoang N, et al. Association of diabetes mellitus and chronic hepatitis C virus infection. Hepatology 1999;29:328–33.
3. Hui JM, Sud A, Farrell GC, et al. Insulin resistance is associated with chronic hepatitis C virus infection and fibrosis progression. Gastroenterology 2003;125:1695–704.
4. Adami HO, Chow WH, Nyren O, et al. Excess risk of primary liver cancer in patients with diabetes mellitus. J Natl Cancer Inst 1996;88:1472–7.
5. El-Serag HB, Tran T, Everhart JE. Diabetes increases the risk of chronic liver disease and hepatocellular carcinoma. 2004;126:460–8.
6. Nagao Y, Kawaguchi T, Tanaka K, et al. Extrahepatic manifestations and insulin resistance in an HCV hyperendemic area. Int J Mol Med 2005;16:291–6.
7. Sumie S, Kawaguchi T, Taniguchi E, et al. Down-regulated SH2-containing inositol phosphatase (SHIP)-2 expression in HCC and hyperinsulinemia are involved in prognosis of men with HCV infection. Hepatology 2005;42:382A.
8. Furutani M, Nakashima T, Sumida Y, et al. Insulin resistance/beta-cell function and serum ferritin level in non-diabetic patients with hepatitis C virus infection. Liver Int 2003;23:294–9.
9. Hickman IJ, Powell EE, Prins JB, et al. In overweight patients with chronic hepatitis C, circulating insulin is associated with hepatic fibrosis: Implications for therapy. J Hepatol 2003;39:1042–8.
10. Knobler H, Zhornicky T, Sandler A, et al. Tumor necrosis factor-alpha-induced insulin resistance may mediate the hepatitis C virus-diabetes association. Am J Gastroenterol 2003;98:2751–6.
11. Zekry A, McHutchison JG, Diehl AM. Insulin resistance and steatosis in hepatitis C virus infection. Gut 2005;54:903–6.
12. Koike K. Hepatitis C as a metabolic disease: Implication for the pathogenesis of NASH. Hepatol Res 2005;33:145–50.
13. Shintani Y, Fujie H, Miyoshi H, et al. Hepatitis C virus infection and diabetes: Direct involvement of the virus in the development of insulin resistance. Gastroenterology 2004;126:840–8.
14. AlDosary AA, Ramji AS, Elliott TG, et al. Post-liver transplantation diabetes mellitus: An association with hepatitis C. Liver Transpl 2002;8:356–61.
15. Kawaguchi T, Yoshida T, Harada M, et al. Hepatitis C virus down-regulates insulin receptor substrates 1 and 2 through up-regulation of suppressor of cytokine signaling 3. Am J Pathol 2004;165:1499–508.
16. Shiratori Y, Imazeki F, Moriyama M, et al. Histologic improvement of fibrosis in patients with hepatitis C who have sustained response to interferon therapy. Ann Intern Med 2000;132:517–24.
17. Yoshida H, Shiratori Y, Moriyama M, et al. Interferon therapy reduces the risk for hepatocellular carcinoma: National surveillance program of cirrhotic and noncirrhotic patients with chronic hepatitis C in Japan. IHIT Study Group. Inhibition of hepatocarcinogenesis by interferon therapy. Ann Intern Med 1999;131:174–81.
18. Matthews DR, Hosker JP, Rudenski AS, et al. Homeostasis model assessment: Insulin resistance and beta-cell function from fasting plasma glucose and insulin concentrations in man. Diabetologia 1985;28:412–9.
19. Okamoto H, Sugiyama Y, Okada S, et al. Typing hepatitis C virus by polymerase chain reaction with type-specific primers: Application to clinical surveys and tracing infectious sources. J Gen Virol 1992;73:673–9.
20. Simmonds P, Holmes EC, Cha TA, et al. Classification of hepatitis C virus into six major genotypes and a series of subtypes by phylogenetic analysis of the NS-5 region. J Gen Virol 1993;74:2391–9.
21. Bedossa P, Poynard T. An algorithm for the grading of activity in chronic hepatitis C. The METAVIR Cooperative Study Group. Hepatology 1996;24:289–93.
22. Kawaguchi T, Sakisaka S, Mitsuyama K, et al. Cholestasis with altered structure and function of hepatocyte tight junction and decreased expression of canalicular multispecific organic anion transporter in a rat model of colitis. Hepatology 2000;31:1285–95.
23. Kawaguchi T, Sakisaka S, Sata M, et al. Different lobular distributions of altered hepatocyte tight junctions in rat models of intrahepatic and extrahepatic cholestasis. Hepatology 1999;29:205–16.
24. Chiles R, Tzagournis M. Excessive serum insulin response to oral glucose in obesity and mild diabetes. Study of 501 patients. Diabetes 1970;19:458–64.
25. Bahtiyar G, Shin JJ, Aytaman A, et al. Association of diabetes and hepatitis C infection: Epidemiologic evidence and pathophysiologic insights. Curr Diab Rep 2004;4:194–8.
26. Kawaguchi T, Nagao Y, Tanaka K, et al. Causal relationship between hepatitis C virus core and the development of type 2 diabetes mellitus in a hepatitis C virus hyperendemic area: A pilot study. Int J Mol Med 2005;16:109–14.
27. Imano E, Kanda T, Ishigami Y, et al. Interferon induces insulin resistance in patients with chronic active hepatitis C. J Hepatol 1998;28:189–93.
28. Ito Y, Takeda N, Ishimori M, et al. Effects of long-term interferon-alpha treatment on glucose tolerance in patients with chronic hepatitis C. J Hepatol 1999;31:215–20.

29. Romero-Gomez M, Del Mar Viloria M, Andrade RJ, et al. Insulin resistance impairs sustained response rate to peginterferon plus ribavirin in chronic hepatitis C patients. Gastroenterology 2005;128:636–41.
30. Yan FM, Chen AS, Hao F, et al. Hepatitis C virus may infect extrahepatic tissues in patients with hepatitis C. World J Gastroenterol 2000;6:805–11.
31. Narita R, Abe S, Kihara Y, et al. Insulin resistance and insulin secretion in chronic hepatitis C virus infection. J Hepatol 2004;41:132–8.
32. Magnusson J, Tranberg KG. Impaired early insulin response to intravenous glucose in alcoholic liver cirrhosis. Scand J Gastroenterol 1987;22:301–7.
33. Matsumoto K, Miyake S, Yano M, et al. Glucose tolerance, insulin secretion, and insulin sensitivity in nonobese and obese Japanese subjects. Diabetes Care 1997;20:1562–8.
34. Lin SY, Wang YY, Sheu WH. Increased serum soluble tumor necrosis factor receptor levels are associated with insulin resistance in liver cirrhosis. Metabolism 2004;53:922–6.

CONFLICT OF INTEREST

Guarantor of the article: Takumi Kawaguchi, M.D., Ph.D.
Financial support:. This study was supported, in part, by a Grant in Aid for Scientific Research (C) (No. 16590648 to M.S.) from the Ministry of Education, Culture, Sports, Science and Technology of Japan, the Vehicle Racing Commemorative Foundation, and the 21st Century COE Program for Medical Science, Kurume University.
Potential competing interests: None

Lipid-Induced Oxidative Stress Causes Steatohepatitis in Mice Fed an Atherogenic Diet

Naoto Matsuzawa,[1,2] Toshinari Takamura,[1] Seiichiro Kurita,[1] Hirofumi Misu,[1] Tsuguhito Ota,[1] Hitoshi Ando,[1] Masayoshi Yokoyama,[1] Masao Honda,[1] Yoh Zen,[3] Yasuni Nakanuma,[3] Ken-ichi Miyamoto,[2] and Shuichi Kaneko[1]

Recently, nonalcoholic steatohepatitis (NASH) was found to be correlated with cardiovascular disease events independently of the metabolic syndrome. The aim of this study was to investigate whether an atherogenic (Ath) diet induces the pathology of steatohepatitis necessary for the diagnosis of human NASH and how cholesterol and triglyceride alter the hepatic gene expression profiles responsible for oxidative stress. We investigated the liver pathology and plasma and hepatic lipids of mice fed the Ath diet. The hepatic gene expression profile was examined with microarrays and real-time polymerase chain reactions. The Ath diet induced dyslipidemia, lipid peroxidation, and stellate cell activation in the liver and finally caused precirrhotic steatohepatitis after 24 weeks. Cellular ballooning, a necessary histological feature defining human NASH, was observed in contrast to existing animal models. The addition of a high-fat component to the Ath diet caused hepatic insulin resistance and further accelerated the pathology of steatohepatitis. A global gene expression analysis revealed that the Ath diet up-regulated the hepatic expression levels of genes for fatty acid synthesis, oxidative stress, inflammation, and fibrogenesis, which were further accelerated by the addition of a high-fat component. Conversely, the high-fat component down-regulated the hepatic gene expression of antioxidant enzymes and might have increased oxidative stress. *Conclusion:* The Ath diet induces oxidative stress and steatohepatitis with cellular ballooning. The high-fat component induces insulin resistance, down-regulates genes for antioxidant enzymes, and further aggravates the steatohepatitis. This model suggests the critical role of lipids in causing oxidative stress and insulin resistance leading to steatohepatitis. (HEPATOLOGY 2007;46:1392-1403.)

Abbreviations: 4-HNE, 4-hydroxy-2-nonenal; α-SMA, α-smooth muscle actin; ALT, alanine aminotransferase; Ath, atherogenic; Ath+HF, atherogenic and high-fat; AUC, area under the curve; BW, body weight; Col1a1, procollagen type I alpha 1; Col1a2, procollagen type I alpha 2; Col4a1, procollagen type IV alpha 1; CPT-1a, carnitine palmitoyltransferase 1a; FAS, fatty acid synthase; FFA, free fatty acid; GPCR, G protein-coupled receptor; GPCRDB, G Protein-Coupled Receptor Database; GTT, glucose tolerance test; H&E, hematoxylin-eosin; HDL-C, high-density lipoprotein-cholesterol; HOMA-IR, homeostasis model assessment of insulin resistance; HPLC, high-performance liquid chromatography; HSC, hepatic stellate cell; IRS, insulin receptor substrate; ITT, insulin tolerance test; LDL, low-density lipoprotein; LDL-C; low-density lipoprotein-cholesterol; MAPK, mitogen-activated protein kinase; MCD, methionine- and choline-deficient; mRNA, messenger RNA; NADPH, reduced-form nicotinamide adenine dinucleotide phosphate; NAFLD, nonalcoholic fatty liver disease; NASH, nonalcoholic steatohepatitis; ND, not determined; PAI-1, plasminogen activator inhibitor 1; PCR, polymerase chain reaction; PPARα, peroxisome proliferator-activated receptor α; ROS, reactive oxygen species; SEM, standard error of the mean; SREBP-1c, sterol regulatory element binding protein 1c; TBS-T, trishydroxymethylaminomethane-buffered saline Tween 20; TCA, tricarboxylic acid cycle; TG, triglyceride; TGF-β, transforming growth factor β; TNF-α, tumor necrosis factor α; VLDL-C, very low density lipoprotein-cholesterol.

From the [1]Department of Disease Control and Homeostasis, Graduate School of Medical Science, [2]Department of Pharmacy and Health Science, Graduate School of Natural Science and Technology, and [3]Department of Human Pathology, Graduate School of Medical Science, Kanazawa University, Kanazawa, Japan.

Received January 9, 2007; accepted June 12, 2007.

Supported by grants-in-aid from the Ministry of Education, Culture, Sports, Science, and Technology of Japan.

Address reprint requests to: Toshinari Takamura, M.D., Ph.D., Department of Disease Control and Homeostasis, Graduate School of Medical Science, Kanazawa University, 13-1 Takara-machi, Kanazawa, Ishikawa 920-8641, Japan. E-mail: ttakamura@m-kanazawa.jp; fax: (81) 76-234-4250.

Published online in Wiley InterScience (www.interscience.wiley.com).

DOI 10.1002/hep.21874

Potential conflict of interest: Nothing to report.

Supplementary material for this article can be found on the HEPATOLOGY Web site (http://interscience.wiley.com/jpages/0270-9139/suppmat/index.html).

Nonalcoholic fatty liver disease (NAFLD) is currently the most common chronic liver condition in the Western world. Clinical, epidemiological, and biochemical data strongly support the concept that NAFLD is the hepatic manifestation of the metabolic syndrome, the constellation of metabolic abnormalities including obesity, dyslipidemia, and insulin resistance.[1] NAFLD includes not only steatosis (without other injury) but also various degrees of inflammation and fibrosis.[2] Simple steatosis is usually considered benign, but the development of inflammatory changes in the liver [called nonalcoholic steatohepatitis (NASH)] is recognized as a precursor to more severe liver disease and sometimes evolves into cryptogenic cirrhosis.[3] It has been recently proposed that NASH is strongly correlated with cardiovascular disease events independently of the metabolic syndrome.[4] Therefore, further investigations of NASH are required to elucidate the pathogenesis of this process and to develop treatments.

To date, however, studies of NASH have been hampered by the absence of a suitable experimental model. The use of genetic defects or targeted overexpression to produce obesity[5] or impaired hepatic lipid metabolism[6] in rodents has been used as an NAFLD model. Although these genetic manipulations can assess the biological importance of each gene *in vivo*, they might not reflect the natural etiology of NAFLD in patients and rarely lead to the pathology of NASH. The other models frequently used are based on nutritional manipulations. Natural nutritional models have been described, including the use of a sucrose-rich and fat-rich diet.[7] However, in these models, rodents accumulate minimal fat and develop subtle inflammation of the liver. The methionine- and choline-deficient (MCD) model, which is frequently used to produce more progressive liver pathology, leads to the development of steatosis with lobular inflammation and with perisinusoidal and pericentral fibrosis.[8,9] However, this model lacks lipotrophic factors, insulin resistance,[10] or the cellular ballooning that is observed only with the addition of a high-fat component to the MCD diet.[11]

In this study, we focused on an atherogenic (Ath) diet, which contains cholesterol and cholic acid. Because the diet produces not only an Ath lipoprotein profile but also vascular fatty streak lesions, it has been widely used to study atherosclerosis in animals, including mice.[12] Although the Ath diet has recently been reported to induce liver steatosis, inflammation, and fibrosis,[13] lipid metabolism, insulin resistance, and hepatic gene expression profiles responsible for liver pathology remain to be determined in this model. To address this issue, we investigated the time course of the pathological changes and gene expression profiles of the liver in mice fed the Ath diet. In addition, by adding a high-fat component to the Ath diet, we elucidated the impact of insulin resistance, which is commonly observed in NASH patients, on the development of oxidative stress in the liver and pathology of steatohepatitis.

Table 1. The Composition of the 3 Diets

Composition	Control	Ath	Ath+HF
CRF-1 (%)	100	90.75	38.25
Cocoa butter (%)	–	7.50	60.0
Cholesterol (%)	–	1.25	1.25
Cholate (%)	–	0.50	0.50
			(wt/wt %)
Energy composition	**Control**	**Ath**	**Ath+HF**
Carbohydrate (g)	60.9	55.2	23.3
Protein (g)	22.4	20.3	8.6
Fat (g)	6.0	14.0	60.0
Total calorie (kcal)	363	411	669
			(/100 g)

The contents of vitamins and minerals in each diet are presented in Supplementary Table 1.

Materials and Methods

Animals and Experimental Design. Male C57Bl/6J mice were purchased from Charles River Laboratories Japan (Yokohama, Japan) at 6 weeks of age. After 2 weeks of acclimation, the mice were divided into the following 3 groups: (1) control mice given a standard chow (CRF-1, Charles River Laboratories Japan), (2) mice given an Ath diet, and (3) mice fed an atherogenic and high-fat (Ath+HF) diet. The Ath and Ath+HF diets were prepared by the addition of cocoa butter, cholesterol, and cholate to CRF-1. These diets were prepared by Oriental Yeast (Tokyo, Japan). The compositions of each diet are shown in Table 1 and Supplementary Table 1. At 6 weeks of age, the mice were housed in colony cages with a 12-hour light/12-hour dark cycle, and they were given food and water *ad libitum*. All animal procedures were in accordance with the standards set forth in the Guidelines for the Care and Use of Laboratory Animals at the Takara-Machi campus of Kanazawa University (Japan).

Blood Sampling and Analysis. At 6, 12, or 24 weeks, blood samples were obtained from the tail vein following a 12-hour fast. Enzymatic assays for the total cholesterol, free cholesterol, free fatty acids (FFAs), triglyceride (TG), and alanine aminotransferase (ALT) were performed with kits purchased from Wako Pure Chemical Industries (Osaka, Japan). The cholesterol and TG profiles in plasma lipoproteins were analyzed with a dual-detection high-performance liquid chromatography (HPLC) system with 2 tandem connected TSKgel LipopropakXL

columns (300 × 7.8 mm; Tosoh, Japan) by Skylight Biotech (Akita, Japan).[14]

Glucose Tolerance Tests (GTTs) and Insulin Tolerance Tests (ITTs). At 12 weeks, GTTs and ITTs were conducted. For GTTs, glucose was administered (1.5 g/kg body weight) following a 12-hour fast. For ITTs, mice were injected intraperitoneally with insulin (0.5 U/kg of body weight; Humulin R, Eli Lilly, Indianapolis, IN) following a 4-hour fast. The glucose values were measured from whole venous blood with a blood glucose monitoring system (FreeStyle, Kissei, Matsumoto, Japan) 0, 15, 30, 60, and 120 minutes after the administration of glucose or insulin.

Pyruvate Challenge Test. At 6 weeks, we conducted the pyruvate challenge test.[15,16] The mice, deprived of food for 16 hours, were injected intraperitoneally with pyruvate dissolved in saline (2 g/kg). The blood glucose values were measured 0, 15, 30, 60, and 90 minutes after the injection of pyruvate.

Tissue Preparation and Histological Examination. At 6, 12, or 24 weeks, the mice were killed by cervical dislocation under diethyl ether anesthesia following a 12-hour fast. The livers were immediately removed and weighed. A large portion of each liver was snap-frozen in liquid nitrogen for later RNA studies. The remaining tissue was fixed in 10% buffered formalin, processed, and embedded in paraffin for hematoxylin-eosin (H&E), Azan, and Sirius red staining and was blindly scored by a single pathologist. Steatosis, fibrosis, and acinar inflammation were semiquantitatively evaluated according to the standard criteria of grading and staging for NASH, with minor modifications.[17] To evaluate steatosis, we used the absolute percentage of the macrovesicular fat droplet area in the section area (that is, 8×10^5 hepatocytes in 4 mm^2). For inflammation, 0 was defined as no hepatocyte injury or inflammation, 1 was defined as mild focal injury, 2 was defined as noticeable injury, and 3 was defined as severe zone 3 hepatocyte injury or inflammation. For fibrosis, 0 was defined as no fibrosis, 1 was defined as pericellular and perivenular fibrosis, 2 was defined as focal bridging fibrosis, 3 was defined as much bridging fibrosis with lobular distortion, and 4 was defined as cirrhosis.

Slides were immunostained with monoclonal mouse anti-human α-smooth muscle actin (α-SMA; Dako Japan, Kyoto, Japan). This was followed by the application of the immunoperoxidase technique with an Envision kit (Dako Japan). The peroxidase activity was identified by a reaction with 3′,3′-diaminobenzidine (Sigma, St Louis, MO). Areas staining for α-SMA were quantified morphometrically with WinROOF version 5.7 (Mitani Shoji, Fukui, Japan) and expressed as percentages of the field area.

Measuring the Hepatic Lipid Content. Hepatic lipids were extracted with chloroform/methanol (2:1) according to a published method.[18] With a kit (Wako), the extract was dissolved in water and subsequently analyzed for TG, total cholesterol, free cholesterol, and FFAs.

Measuring the Hepatic Hydroxyproline Content. The hydroxyproline content in liver samples was quantified colorimetrically according to a published method.[19] Briefly, a 0.2-g liver sample was homogenized in 6 N HCl and hydrolyzed at 110°C for 16 hours. The hydrolysate was filtered, aliquots were evaporated under a vacuum, and the sediment was redissolved in 50% isopropanol. Then, the samples were incubated in a solution containing 0.84% chloramine-T, 42 mM sodium acetate, 2.6 mM citric acid, and 39.5% (vol/vol) isopropanol (pH 6.0) for 10 minutes at room temperature. Next, the samples were incubated in a solution containing 0.248 g of *p*-dimethylaminobenzaldehyde dissolved in 0.27 mL of 60% perchloric acid and 0.73 mL of isopropanol for 90 minutes at 50°C. The hydroxyproline content was quantified photometrically at 558 nm.

Measuring Hepatic Protein Carbonyls. The concentration of hepatic proteins containing carbonyl groups (those that react with 2,4-dinitrophenylhydrazine to form the corresponding hydrazone) was determined spectrophotometrically according to the instructions with a protein carbonyl assay kit (Cayman Chemical, Ann Arbor, MI).

RNA Preparation for the Microarray Analysis. Total RNA was isolated from the frozen liver with the TOTALLY RNA kit (Applied Biosystems, Foster City, CA). Each sample was prepared by equal amounts of total RNA being pooled from 3 mice in the same group. Three micrograms of total RNA was used to synthesize antisense RNA with the AminoAllyl MessageAmp II antisense RNA kit (Applied Biosystems) for oligo-microarrays (AceGene Mouse Oligo Chip 30K, DNA Chip Research, Yokohama, Japan). Each microarray hybridization sample and the reference amino allyl antisense RNA were labeled with Cy5 and Cy3, respectively. Hybridization and washing were performed according to the manufacturer's instructions; this was followed by scanning with a G2505B microarray scanner (Agilent Technologies, Palo Alto, CA) and then image analysis with GenePix Pro 4.1 software (Axon Instruments, Union City, CA). Microarray data were normalized (LOWESS [locally weighted polynomial regression] method) with GeneSpring version 7.2 software (Agilent Technologies). For the pathway analysis, we used the GenMAPP and MAPPFinder software package.[20,21] The GenMAPP program contains

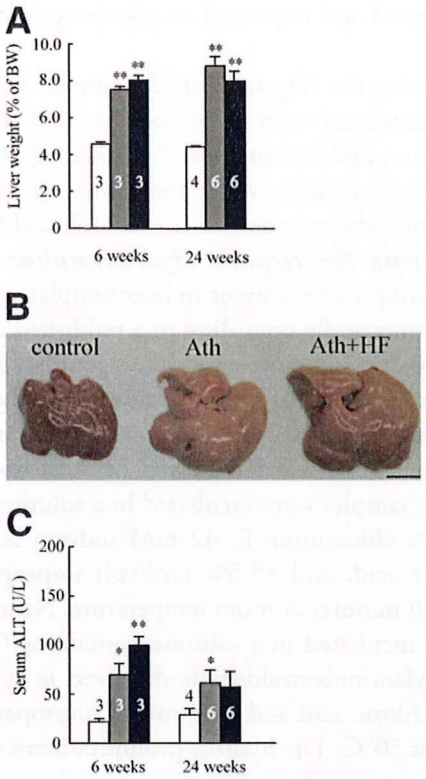

Fig. 1. Effects of 3 diets on the liver weight and morphology and serum ALT. (A) Liver weight with respect to the body weight (BW) of control mice fed standard chow (white bars), the Ath diet (gray bars), or the Ath+HF diet (black bars) after 6 or 24 weeks. (B) Photograph of livers after 12 weeks of feeding with the standard chow, Ath diet, or Ath+HF diet (scale bars: 10 mm). (C) Serum ALT levels after 6 or 24 weeks. The values represent the means ± the SEM. The number of animals per group is indicated in or just above the bars. $*P < 0.05$ and $**P < 0.01$ versus the control group.

many pathway maps that can be associated with imported microarray data. The MAPPFinder program, which links gene expression data to the pathway maps, can calculate the z score (standardized difference score) and the percentage of genes measured that meet user-defined criteria (±25% in the change fold in our analysis). With the z score and the percentage, the pathways were ranked according to the relative change in the gene expression. The microarray data sets have been submitted to the Genome Expression Omnibus Database (available at http://www.ncbi.nlm.nih.gov/geo/) under series GSE5852.

Quantitative Real-Time Polymerase Chain Reaction (PCR). The reverse transcription of 100 ng of total RNA (the same sample used for the microarray analysis) was performed with Oligo(dT)$_{12\text{-}18}$ primer and SuperScript III reverse transcriptase (Invitrogen, Carlsbad, CA). PCR was performed on an ABI-Prism 7900HT (Applied Biosystems). The specific PCR primers and TaqMan probe used in this study were obtained from Applied Biosystems. The PCR conditions were 1 cycle at 50°C for 2 minutes and at 95°C for 10 minutes followed by 40 cycles at 95°C for 15 s and at 60°C for 1 minute.

Western Blot Analysis. Livers were homogenized in a buffer containing 20 mM trishydroxymethylaminomethane-HCl (pH 7.5), 5 mM ethylene diamine tetraacetic acid, 1% NP-40, and a protease inhibitor cocktail (Pierce, Rockford, IL). Homogenated proteins (30 μg/lane) were separated by 4%-20% gradient sodium dodecyl sulfate–polyacrylamide gels (Daiichi Chemicals, Tokyo, Japan) and resolved with 130 V over 2 hours. Proteins were transferred to polyvinylidene difluoride membranes (Millipore, Billerica, MA) with a Transblot apparatus (Bio-Rad, Hercules, CA). The membranes were blocked in a buffer containing 5% nonfat milk, 50 mM trishydroxymethylaminomethane (pH 7.6), 150 mM NaCl, and 0.1% Tween 20 [trishydroxymethylaminomethane-buffered saline Tween 20 (TBS-T)] for 12 hours at 4°C. They were then probed with the monoclonal anti–4-hydroxy-2-nonenal (4-HNE) antibody (NOF, Tokyo, Japan) at a 1:200 dilution, with the polyclonal anti–insulin receptor substrate 2 (IRS-2) antibody (Millipore) at a 1:500 dilution, or with the polyclonal anti–glyceraldehyde 3-phosphate dehydrogenase antibody (Santa Cruz Biotechnology, Santa Cruz, CA) at a 1:3000 dilution in 5% bovine serum albumin TBS-T for 12 hours at 4°C. After the membranes had been washed in TBS-T, the blots were incubated with the horseradish peroxidase–linked secondary antibody (Cell Signaling Technology, Beverly, MA). Signals were detected with a chemiluminescence detection system (ECL Plus, GE Healthcare Bio-Sciences, Piscataway, NJ) and exposure to X-ray film. The hepatic 4-HNE contents were quantified with WinROOF version 5.7 (Mitani Shoji).

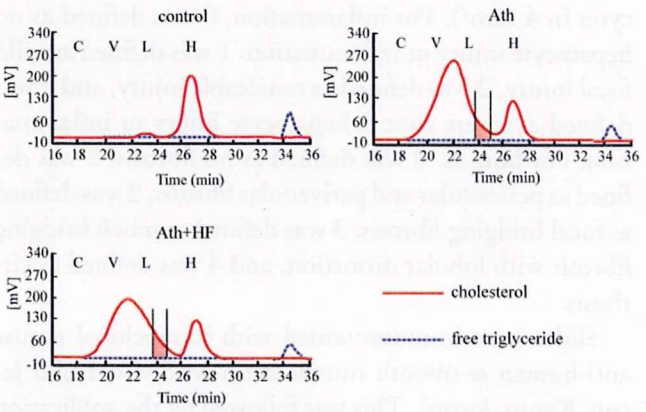

Fig. 2. HPLC analysis of plasma lipoproteins: fractionation by HPLC of cholesterol and free TG from mouse plasma after 24 weeks on the diet. The chromatograms for 1 representative sample are presented. The chylomicron, VLDL-C, LDL-C, and HDL-C fractions are labeled C, V, L, and H, respectively. The shaded fractions correspond to the level of small dense LDL-C.

Table 2. Effects of the 3 Diets on Body Weight and Lipid Levels at 6 or 24 Weeks of Feeding

	6 weeks			24 weeks		
Diet type	Control (n = 3)	Ath (n = 3)	Ath+HF (n =3)	Control (n = 4)	Ath (n = 6)	Ath+HF (n = 6)
Body weight (g)	24.7 ± 0.5	24.9 ± 0.4	23.2 ± 0.4	29.0 ± 0.7	28.1 ± 1.8	26.4 ± 1.1**
Epididymal fat pad weight (g)	0.14 ± 0.01	0.15 ± 0.01	0.15 ± 0.02	0.25 ± 0.01	0.09 ± 0.01**	0.17 ± 0.01**
Plasma triglycerides (mg/dL)	68.0 ± 5.2	54.6 ± 10.1	24.0 ± 3.6**	41.5 ± 4.6	33.8 ± 3.5	20.8 ± 1.7*
Plasma total cholesterol (mg/dL)	85.0 ± 8.5	173.6 ± 5.3**	168.1 ± 5.3**	84.6 ± 3.8	257.1 ± 10.8**	204.4 ± 8.8**
Plasma free cholesterol (mg/dL)	23.9 ± 2.2	45.9 ± 2.7**	40.2 ± 0.7**	17.3 ± 0.3	47.5 ± 5.6**	31.3 ± 2.3*
Plasma FFA (mEq/L)	0.58 ± 0.09	0.75 ± 0.10	0.46 ± 0.07	0.48 ± 0.04	0.48 ± 0.04	0.24 ± 0.06*
Plasma insulin (μU/mL)	N.D.	N.D.	N.D.	6.2 ± 0.3	11.2 ± 1.7	13.8 ± 2.9
Fasting blood glucose (mg/dL)	N.D.	N.D.	N.D.	93 ± 4	85 ± 4	93 ± 8
HOMA-IR	N.D.	N.D.	N.D.	1.4 ± 0.1	2.3 ± 0.3	3.1 ± 0.4*
Hepatic triglycerides (μg/mg protein)	67.2 ± 10.4	89.3 ± 19.7	150.8 ± 21.6*	148.6 ± 20.9	52.8 ± 17.4*	64.5 ± 9.2*
Hepatic total cholesterol (μg/mg protein)	42.0 ± 2.8	206.8 ± 22.5**	342.8 ± 40.8**	34.3 ± 2.2	143.5 ± 24.1*	192.8 ± 25.0**
Hepatic free cholesterol (μg/mg protein)	22.1 ± 3.9	30.4 ± 4.2	52.6 ± 6.6*	19.9 ± 2.3	33.0 ± 2.6*	30.9 ± 5.9
Hepatic FFA (μEq/mg protein)	45.6 ± 4.0	52.6 ± 3.3	63.0 ± 2.8*	53.1 ± 1.8	81.1 ± 6.3*	83.6 ± 8.7*

Data are means ± SEM. Significantly different from control value: *$P < 0.05$; **$P < 0.01$. Abbreviations: FFA, free fatty acid; HOMA-IR, homeostasis model assessment insulin resistance; N.D., Not determined.

Statistical Analysis. The results are shown as the means ± the standard error of the mean (SEM). The data were analyzed with a 1-way analysis of variance to compare the means of all groups. The Bonferroni multiple-comparison procedure was used to determine which pairs of means were different. Differences in the histological scores between the Ath and Ath+HF groups were compared with the Mann-Whitney U test. All calculations were performed with SPSS version 12.0 software for Windows (SPSS, Chicago, IL).

Results

Ath Diet Causes Hepatomegaly and Liver Injury. Hepatomegaly was observed in the Ath and Ath+HF groups (Fig. 1A). As shown in Fig. 1B, the livers of mice fed the Ath diet were grossly enlarged and pale in color. The serum ALT level was also elevated in the Ath and Ath+HF groups (Fig. 1C). Splenomegaly, frequently associated with cirrhosis, was detected in the Ath and Ath+HF groups at 24 weeks.

Effect of the Ath Diet on the Plasma Lipid Levels and Hepatic Lipid Content. As shown in Table 2, the plasma cholesterol levels were significantly elevated in the Ath diet group after both 6 and 24 weeks. An HPLC analysis revealed that the Ath and Ath+HF diets markedly increased the very low density lipoprotein-cholesterol (VLDL-C), low-density lipoprotein-cholesterol (LDL-C), and small dense LDL-C fractions, whereas they lowered high-density lipoprotein-cholesterol (HDL-C) in comparison with the controls (Fig. 2). As reported previously, we also confirmed atherosclerotic lesions in the mice fed the Ath and Ath+HF diets but not in the mice fed normal chow (data not shown).

The Ath and Ath+HF diets accumulated cholesterol in the liver after both 6 and 24 weeks. In addition to cholesterol, TG and FFA also accumulated with the Ath+HF diet. In comparison with hepatic lipid levels after 6 weeks, cholesterol and TG decreased in the livers of mice fed the Ath and Ath+HF diets after 24 weeks, and this indicated the progression of extensive hepatic fibrosis and impaired hepatocellular function. As is often found in patients with advanced liver disease, the serum ALT levels decreased with the progression of hepatic fibrosis, probably because of the impaired regeneration of hepatocytes and the production of ubiquitous liver enzymes.[22]

Effects of the Ath Diet on Systemic or Hepatic Insulin Resistance. GTT and ITT after 12 weeks showed that the mice fed the Ath diet were remarkably sensitive to insulin (Fig. 3A,B). This ameliorating effect on the glucose tolerance and insulin sensitivity may be attributable to decreased adipose tissue in the mice fed the Ath or Ath+HF diet (Table 2). Therefore, we next evaluated the hepatic insulin sensitivity. For this purpose, we performed the pyruvate challenge test, an established method for evaluating hepatic insulin sensitivity,[15,16] by investigating the rise in blood glucose in response to the administration of pyruvate, a precursor for gluconeogenesis. The mice fed the Ath+HF diet showed an increased rise in the blood glucose concentration after pyruvate injection (Fig. 3C) compared with the mice fed the standard chow, and this suggested that the Ath+HF diet causes hepatic insulin resistance. Furthermore, as shown in Table 2, the homeostasis model assessment of insulin resistance (HOMA-IR) was significantly higher in the mice fed the Ath+HF diet than in the control mice. The expression of messenger RNA (mRNA) for phosphoenolpyruvate carboxykinase, the rate-controlling enzyme of

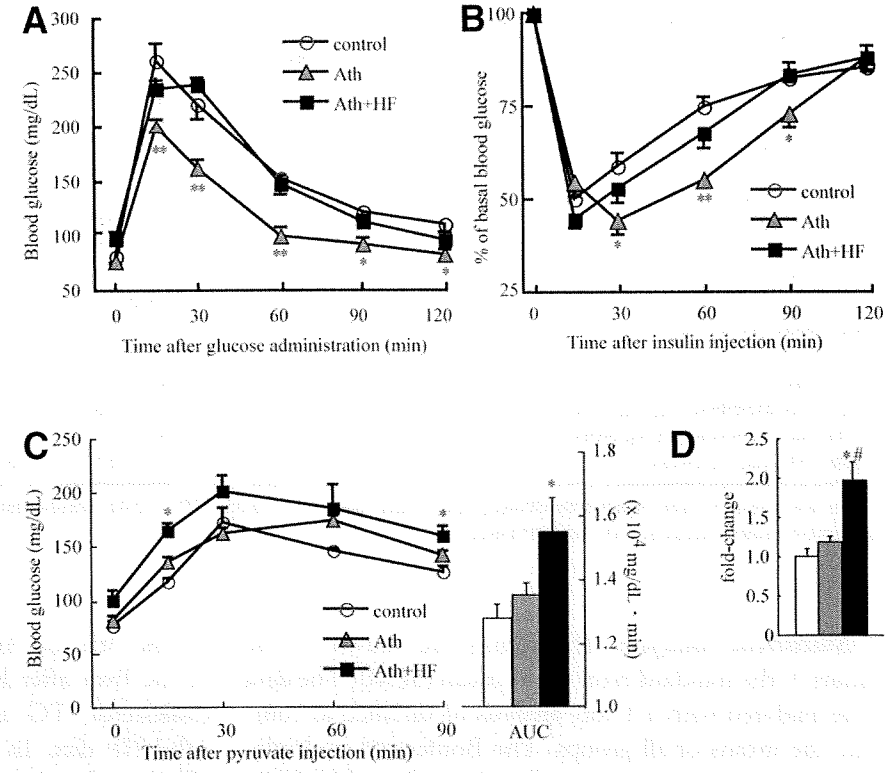

Fig. 3. Evaluation of glucose tolerance and insulin sensitivity. (A) GTT and (B) ITT after 12 weeks on standard chow (n = 4), the Ath diet (n = 5), or the Ath+HF diet (n = 5). (C) Pyruvate challenge test after 6 weeks on standard chow (n = 4), the Ath diet (n = 4), or the Ath+HF diet (n = 4). The area under the curve (AUC) of the blood glucose levels during the pyruvate challenge test was calculated. (D) mRNA levels of phosphoenolpyruvate carboxykinase genes in the livers of mice fed standard chow (white bar; n = 3), the Ath diet (gray bar; n = 3), or the Ath+HF diet (black bar; n = 3) after 12 weeks. The gene expression was normalized with eukaryotic 18S ribosomal RNA. The degree of change in the gene expression was based on the mean expression levels in control mice. The values represent the means ± the SEM. $*P < 0.05$ and $**P < 0.01$ versus the control group. $\#P < 0.05$ versus the Ath group.

gluconeogenesis for which the expression is negatively regulated by insulin, was significantly higher in the mice fed the Ath+HF diet than in the control mice (Fig. 3D). These results suggest that the Ath+HF diet causes hepatic insulin resistance.

Ath Diet Induces Steatosis, Fibrosis, and Cellular Ballooning of the Liver. Figure 4 shows the time course of histological changes in the livers of mice fed the Ath or Ath+HF diet. The Ath diet induced progressive steatosis, inflammation, and fibrosis in a time-dependent manner from 6-24 weeks. Moreover, cellular ballooning, an important histological feature for the diagnosis of human NASH, was observed in the Ath group after 24 weeks. The addition of a high-fat component to the Ath diet accelerated the development of steatosis, inflammation, and fibrosis. Furthermore, before the Ath group, cellular ballooning was already observed in the Ath+HF group after 12 weeks. The hepatic hydroxyproline content, an indicator of collagen accumulation in the liver, increased significantly in the mice fed the Ath diet and increased further in the mice fed the Ath+HF diet (Fig. 4C). Therefore, the Ath diet induces steatohepatitis, and the addition of a high-fat component exacerbates the histological severity of steatohepatitis and hepatic insulin resistance.

High-Fat Component Further Enhances the Activation of Hepatic Stellate Cells (HSCs) with the Ath Diet. The major sources of collagen and other extracellular matrix proteins in liver fibrosis are HSCs.[23] In response to stimuli such as oxidative stress and inflammatory cytokines, HSCs become activated and transform into proliferative fibrogenic cells.[24] We performed an immunohistochemical analysis of α-SMA, an activated HSC marker, at different times. Representative photomicrographs of liver sections stained with the anti–α-SMA antibody are shown in Fig. 5A. We quantified the areas in the liver sections positive for α-SMA morphometrically in the 3 groups at different times as described (Fig. 5A, lower panel). The activation of HSCs was promoted in the livers of mice fed the Ath diet in a time-dependent manner from 6-24 weeks and was further accelerated by the addition of a high-fat component to the Ath diet.

To evaluate oxidative stress causing HSC activation, we assayed proteins modified with 4-HNE, which is a major aldehyde end product of membrane lipid peroxidation due to oxidative stress (Fig. 5B). In concert with the increase in α-SMA–positive cells, 4-HNE–modified proteins accumulated in the livers of mice fed the Ath diet and further accumulated in those of mice fed the Ath+HF diet. In addition to 4-HNE–modified proteins, hepatic protein carbonyls, another marker of oxidative stress, also increased with the Ath and Ath+HF diets (Fig. 5C). These results are consistent with the observation that the Ath+HF diet induced more severe inflammation and fibrosis than the Ath diet.

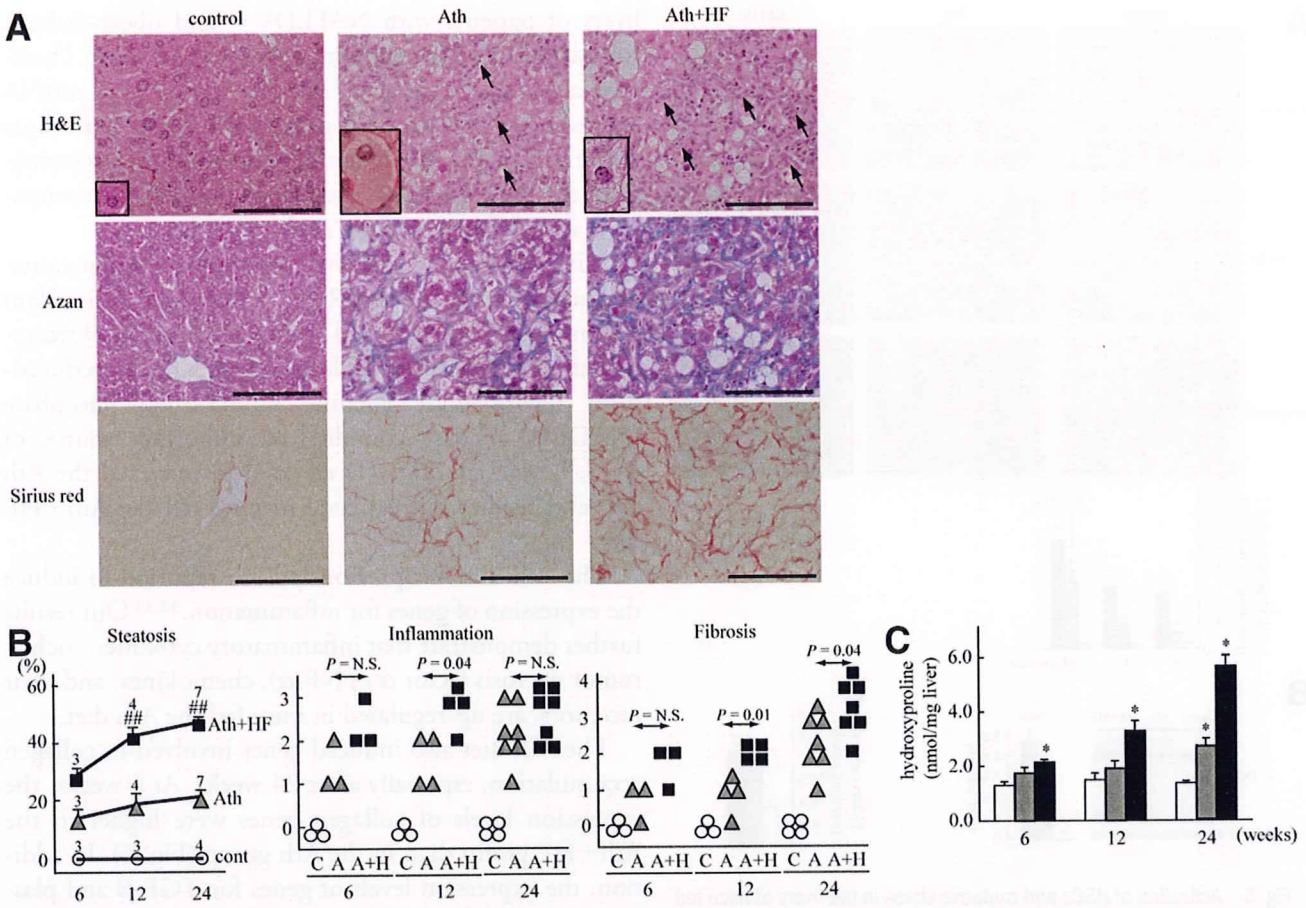

Fig. 4. Representative liver histology, scoring, and occurrence of hepatocyte ballooning. (A) Liver sections were stained with H&E, Azan, and Sirius red after 6, 12, and 24 weeks. The arrows indicate infiltration of the inflammatory cells in the hepatic parenchyma. The characteristic initial pattern of fibrosis in steatohepatitis is collagen deposition, as identified by blue and red staining. The original magnification was ×200. The scale bars represent 10 μm. Ballooning hepatocytes were seen only in the Ath and Ath+HF groups (shown in the inset). (B) The absolute percentage of the macrovesicular fat droplet area in the H&E-stained area was determined to evaluate steatosis. The values represent the means ± the SEM. The number of animals per group is indicated just above the points. ##$P < 0.01$ versus the Ath group. Inflammation and fibrosis scores were assigned in a blinded fashion to H&E-stained samples for inflammation and to Azan-stained samples for fibrosis. The criteria for each score are described in the Materials and Methods section. Differences in the inflammation and fibrosis histological scores between the Ath and Ath+HF groups were compared with the Mann-Whitney U test. The control, Ath, and Ath+HF groups are labeled C (white circles), A (gray triangles), and A+H (black squares), respectively. (C) The hydroxyproline content was determined in the livers of mice fed standard chow (white bars; n = 3), the Ath diet (gray bars; n = 3), or the Ath+HF diet (black bars; n = 3) at 6, 12, and 24 weeks. The values represent the means ± the SEM. **$P < 0.01$ versus the control group. ##$P < 0.01$ versus the Ath group.

Gene Expression in the Livers of Mice Fed the Ath Diet. To address the molecular basis of Ath diet–induced steatohepatitis, we performed a microarray analysis, using livers at early (6 weeks) and precirrhosis stages (24 weeks) in the development of steatohepatitis. We screened 103 pathways determined with GenMAPP and extracted the metabolic pathways significantly altered in the livers of the mice fed the Ath and Ath+HF diets (Table 3). In the livers of the mice fed the Ath diet, genes involved in the inflammatory response and p38 mitogen-activated protein kinase (MAPK) signaling pathway were up-regulated significantly, whereas genes involved in fatty acid β-oxidation were down-regulated significantly in the early stage (6 weeks), and this was followed by coordinated up-regulation of the genes involved in fibrogenesis, such as the transforming growth factor β (TGF-β) signaling pathway, in the late stage (24 weeks). Adding the high-fat component to the Ath diet accelerated the up-regulation of the genes involved in inflammation (electron-transport chain, p38 MAPK signaling pathway, and Fas pathway and stress induction) and fibrogenesis (TGF-β signaling pathway and matrix metalloproteinases). Of these pathways altered in the models, we present the expression levels of representative genes involved in lipid metabolism, inflammation, oxidative stress, and fibrogenesis in Fig. 6 and Supplementary Table 2.

In the livers of mice fed the Ath diet, the expression of genes for fatty acid synthesis, such as sterol regulatory